Unchanged PM2.5 levels over Europe during COVID-19 were buffered by ammonia

Nikolaos Evangeliou[1,*], Ondřej Tichý[2], Marit Svendby Otervik[1], Sabine Eckhardt[1], Yves Balkanski[3], Didier A. Hauglustaine[3]

[1] NILU, Department for Atmospheric & Climate Research (ATMOS), 2007 Kjeller, Norway.

[2] The Czech Academy of Sciences, Institute of Information Theory and Automation, Prague, Czech Republic.

[3] Laboratoire des Sciences du Climat et de l'Environnement (LSCE), CEA-CNRS-UVSQ, 91191, Gif-sur-Yvette, France.

***** Corresponding author: N. Evangeliou (Nikolaos.Evangeliou@nilu.no)

Abstract

The coronavirus outbreak in 2020 had devastating impact on human life, albeit a positive effect for the environment reducing emissions of primary aerosols and trace gases and improving air quality. In this paper, we present inverse modelling estimates of ammonia emissions during the European lockdowns of 2020 based on satellite observations. Ammonia has a strong seasonal cycle and mainly originates from agriculture. We further show how changes in ammonia levels over Europe, in conjunction with decreases in traffic-related atmospheric constituents modulated PM2.5. The key result of this study is a -9.8% decrease in ammonia emissions in the first half of 2020 compared to the same period in 2016–2019 attributed to restrictions related to the global pandemic. We further calculate the delay in the evolution of the ammonia emissions in 2020 before, during and after lockdowns, by a sophisticated comparison of the evolution of ammonia emissions during the same time periods for the reference years (2016–2019). Our analysis demonstrates a clear delay in the evolution of ammonia emissions of -77 kt, that was mainly observed in the countries that suffered the strictest travel, social and working measures. Despite the general drop in emissions during the first half of 2020 and the delay in the evolution of the emissions during the lockdown period, satellite and ground-based observations showed that the European levels of ammonia increased. On one hand, this was due to the reduction of SO_2 and NO_x (precursors of the atmospheric acids with which ammonia reacts) that caused less binding and thus less chemical removal of ammonia (smaller loss – higher lifetime); on the other, the majority of the emissions persisted, because ammonia mainly originates from agriculture, a primary production sector that was influenced slightly by the lockdown restrictions. Despite the projected drop in various atmospheric aerosols and trace gases, PM2.5 levels stayed unchanged or even increased in Europe, due to a number of reasons attributed to the complicated NH_3 - H_2SO_4 - HNO_3 system. Higher water vapour during the European lockdowns favoured more sulfate production from SO_2 and OH (gas phase) or O_3 (aqueous phase). Ammonia first reacted with sulfuric acid also producing sulfate. Then, the continuously accumulating free ammonia reacted with nitric acid shifting the equilibrium reaction towards particulate nitrate. In high free ammonia atmospheric conditions such as those in Europe during the 2020 lockdowns, a small reduction of NO_x levels drives faster oxidation toward nitrate and slower deposition of total inorganic nitrate causing high secondary PM2.5 levels.

1 Introduction

Ammonia (NH3), the most abundant gas, has played a vital role in the evolution of human population through the Haber–Bosch process (Chen et al., 2019). However, today it is recognized to have significant negative influence, not only for the environment (Stevens et al., 2010), but also for human population (Cohen et al., 2017; Pope and Dockery, 2006) and the climate (De Vries et al., 2011). As an alkaline molecule, ammonia regulates the pH of clouds, while its excessive atmospheric deposition and terrestrial runoff affect natural reservoirs creating algae blooms and degrading water quality (Camargo and Alonso, 2006; Krupa, 2003). When emitted to the atmosphere, it reacts with the abundant sulfuric and nitric acids (Malm, 2004) forming sulfate, nitrate, and ammonium and contributing up to 50% to the total aerosol mass (Anderson et al., 2003). The latter has implications for human health (Gu et al., 2014) as aerosols penetrate the human respiratory system and accumulate in the lungs (Pope III et al., 2002) causing premature mortality (Lelieveld et al., 2015). Furthermore, through secondary aerosol formation (Pozzer et al., 2017), ammonia has a significant impact (i) on regional climate (Bellouin et al., 2011) causing visibility problems and contributing to haze effect, and (ii) on global climate directly by scattering incoming radiation (Henze et al., 2012) and indirectly as cloud condensation nuclei (Abbatt et al., 2006) altering the Earth's radiative balance.

The largest portion of atmospheric ammonia originates from the synthesis of nitrogen fertilizers, which are in high demand for agriculture (Erisman et al., 2007). The expansion of intensive agriculture during the 20th century has increased atmospheric ammonia above natural levels (Erisman et al., 2008), while the projected growth of the global population will likely create larger nutritional needs that are expected to further increase ammonia emissions during the 21st century (Pai et al., 2021). Other sources of ammonia include emissions from livestock (Sutton et al., 2000a), industry, ammonia-rich watersheds (Sørensen et al., 2003), traffic (Kean et al., 2009), sewage (Reche et al., 2012), humans (Sutton et al., 2000b), biomass and domestic combustion (Sutton et al., 2008; Fowler et al., 2004) and volcanic eruptions (Sutton et al., 2008).

In the past years, atmospheric ammonia observations were mostly limited to ground-based measurements with relatively sparse monitoring networks. This resulted in large emission uncertainties in regions poorly covered by measurements (Heald et al., 2012). Today, satellite products are capable to record daily ammonia column concentrations providing useful information on its atmospheric abundance. Recently, Van Damme et al. (2021) analyzed Infrared Atmospheric Sounding Interferometer (IASI) retrievals and showed increased ammonia levels over most of Europe after 2015. Then, suddenly the COVID-19 outbreak came in 2020 creating a unique situation (Baekgaard et al., 2020), which affected all segments of life in a detrimental way (Chakraborty and Maity, 2020; Sohrabi et al., 2020). As a measure to inhibit further spread of the virus, authorities took

strict social, travel and working restrictions for months, which resulted in lower traffic-related emissions and improved air quality (Bauwens et al., 2020; Dutheil et al., 2020; Sicard et al., 2020). Illustrating the impact on emissions, Guevara et al. (2021) reported average emission reductions in Europe to be 33% for NO_x, 8% for non-methane volatile organic compounds (NMVOCs), and 7% for SO_x during the strictest lockdowns in 2020, while more than 85% of the total reduction is attributed to road transport. CO_2 emissions were also decreased by 11% over Europe during the first lockdowns (Diffenbaugh et al., 2020), so as aerosols did; notably Black Carbon (BC) emissions dropped by 11% (Evangeliou et al., 2020) and Aerosol Optical Depth (AOD) decreased up to 20% over Central and Northern Europe (Acharya et al., 2021).

While the COVID-19 lockdown impact on emissions for primary aerosols and trace gases has been studied extensively, how ammonia emissions were affected in Europe is unknown. The latter is very important and may have largely moderated the atmospheric levels of particulate matter (Giani et al., 2020; Guevara et al., 2021; Matthias et al., 2021), because of ammonia's contribution to secondary PM2.5 (particulate matter) formation (Anderson et al., 2003). Here, we make use of satellite measurements of ammonia and a novel inversion algorithm to track how ammonia emissions changed before, during and after the European lockdowns in 2020. We examine the reasons behind the estimated changes and validate the results against ground-based observations from the EMEP measurement network (https://emep.int/mscw/, **Figure S *1***). Finally, we calculate the resulting impact of ammonia changes during the European lockdowns on the formation of PM2.5 using a chemistry transport model (CTM) and try to interpret the mechanisms governing these changes.

2 Methods

2.1 Cross-Track Infrared Sounder (CrIS) ammonia measurements

The CrIS sensor onboard the NASA Suomi National Polar-orbiting Partnership provides atmospheric soundings at high spectral resolution (0.625 cm-1) (Shephard et al., 2015) resulting in improved vertical sensitivity for ammonia at the surface (Zavyalov et al., 2013). The CrIS fast physical algorithm (Shephard and Cady-Pereira, 2015) retrieves ammonia at 14 vertical levels using a physics-based optimal estimation retrieval, which also provides the vertical sensitivity (averaging kernels) and an estimate of the retrieval errors (error covariance matrices) for each measurement. Shephard et al. (2020) reports a total column random measurement error of 10–15%, with total random errors of ~30%. The individual profile random errors are 10–30%, while total profile random errors increase above 60% due to the limited vertical resolution (Shephard et al., 2020). Vertical sensitivity and error calculations are also important when using CrIS observations in satellite inverse modelling applications (Li et al., 2019; Cao et al., 2020) as a satellite observational operator can be

generated in a robust manner (see next sections). The detection limit of CrIS measurements has been calculated down to 0.3–0.5 ppbv (Shephard et al., 2020) and the product has been validated extensively against ground-based observations (Dammers et al., 2017; Kharol et al., 2018) showing small differences and high correlations.

Daily CrIS ammonia satellite measurements (version 1.6.2) were gridded on 0.5°×0.5° covering all Europe (10°W–50°E, 25°N–75°N) from 1st January to 30th June 2020. Data were screened prior to its use with Quality Flag ≥ 4, as recommended in the CrIS documentation, and Cloud Flag ≠ 1. The latter excludes retrievals that are performed under thin cloud conditions and are not as reliable as retrievals performed under cloud-free conditions (White et al., 2023). Gridding was chosen to limit the large number of observations (around 10,000 per day per vertical level for 2550 retrievals January to June 2020), hence the need for a large number of source-receptor matrices (SRMs), which is computationally inefficient. Specifically, day and night-time observations from CrIS were averaged in each 0.5° resolution grid-cell daily from 1st January to 30th June 2020. This gridding method, although simple, it gives more robust results than classic interpolation methods and presents small standard deviations of the gridded values (see Tichý et al., 2023). Sitwell and Shephard (2021) showed that the averaging kernels of CrIS ammonia are significant only for the lowest six levels (the upper eight have no influence into the satellite observations) and therefore we have considered these six vertical levels (~1018-619 hPa).

2.2 Source-receptor matrix (SRM) calculations

SRMs were calculated for each 0.5°×0.5° grid-cell over Europe (10°W–50°E, 25°N–75°N) using the Lagrangian particle dispersion model FLEXPART version 10.4 (Pisso et al., 2019) adapted to model ammonia. The model releases computational particles that are tracked backward in time using hourly ERA5 (Hersbach et al., 2020) assimilated meteorological analyses from the European Centre for Medium-Range Weather Forecasts (ECMWF) with 137 vertical layers and a horizontal resolution of 0.5°×0.5°. FLEXPART simulates turbulence (Cassiani et al., 2015), unresolved mesoscale motions (Stohl et al., 2005) and convection (Forster et al., 2007). SRMs were calculated for 7 days backward in time, at temporal intervals that matched satellite measurements and at spatial resolution of 0.5°×0.5°. This 7-day backward tracking is sufficiently long to include almost all ammonia sources that contribute to surface concentrations at the receptors given a typical atmospheric lifetime of about a day (Evangeliou et al., 2021; Van Damme et al., 2018).

The complicated heterogeneous chemistry of ammonia was modelled with the Eulerian model LMDz-OR-INCA, which couples the LMDz (Laboratoire de Météorologie Dynamique) General Circulation Model (GCM) (Hourdin et al., 2006) with the INCA (INteraction with Chemistry and Aerosols) model (Folberth et al., 2006; Hauglustaine et al., 2004) and with the land surface dynamical

vegetation model ORCHIDEE (ORganizing Carbon and Hydrology In Dynamic Ecosystems) (Krinner et al., 2005). The model has a horizontal resolution of 2.5°×1.3°, and 39 hybrid vertical levels extending to the stratosphere. It accounts for large-scale advection of tracers (Hourdin and Armengaud, 1999), deep convection (Emanuel, 1991), while turbulent mixing in the planetary boundary layer (PBL) is based on a local second-order closure formalism. The model simulates atmospheric transport of natural and anthropogenic aerosols and accounts for emissions, transport (resolved and sub-grid scale), and dry and wet (in-cloud/below-cloud scavenging) deposition of chemical species and aerosols interactively. LMDz-OR-INCA includes a full chemical scheme for the ammonia cycle and nitrate particle formation, as well as a state-of-the-art $CH_4/NO_x/CO/NMHC/O_3$ tropospheric photochemistry (Hauglustaine et al., 2014). The global transport of ammonia was simulated for 2020 with a month of spin-up by nudging the winds of the 3-hourly ERA5 (Hersbach et al., 2020) with a relaxation time of 10 days (Hourdin et al., 2006).

For the calculation of ammonia's lifetime, LMDz-OR-INCA ran with traditional emissions for anthropogenic, biomass burning and oceanic emission sources from ECLIPSEv5 (Evaluating the CLimate and Air Quality ImPacts of Short-livEd Pollutants), GFED4 (Global Fire Emission Dataset) and GEIA (Global Emissions InitiAtive) (hereafter called "EGG") (Bouwman et al., 1997; Giglio et al., 2013; Klimont et al., 2017). FLEXPART uses the exponential mass removal for radioactive species based on the e-folding lifetime (Pisso et al., 2019), which gives the time needed to reduce the species mass to 1/e contribution. We calculated the e-folding lifetime (Kristiansen et al., 2016; Croft et al., 2014) of ammonia from LMDz-OR-INCA, assuming that the loss occurs as a result of all processes affecting ammonia (chemical reactions, deposition) with a minimum time-step of 1800 s. Then we calculated the exponential loss of ammonia and the respective loss-rate constant κ (s^{-1}). We point to Tichý et al. (2023) for more details on the methodology to avoid repetition.

Ammonia has a complicated atmospheric chemistry and may react with sulfuric and nitric acid producing sulfate and nitrate. However, under certain atmospheric conditions, the equilibrium reaction with nitric acid can be shifted to the left producing free ammonia (Seinfeld and Pandis, 2000). Tichý et al. (2023) showed that production of free ammonia happened very rarely in continental Europe in 2013–2020 period. Nevertheless, we have previously published a full validation of the obtained CTM concentrations against all the available ground-based measurements of ammonia globally (Tichý et al., 2023), from the EMEP network (https://emep.int/mscw/) in Europe, EANET (East Asia acid deposition NETwork) in Southeastern Asia (https://www.eanet.asia/) and AMoN (Ammonia Monitoring Network in the US, AMoN-US; National Air Pollution Surveillance Program (NAPS) sites in Canada) in North America (http://nadp.slh.wisc.edu/data/AMoN/) .

2.3 Inverse modelling of ammonia emissions

The proposed inversion method is based on a comparison of the CrIS satellite observations with the model profile retrievals to estimate the spatiotemporal ammonia emissions. The comparison of remote-sense observations such as CrIS with model (or in-situ) profiles is not straightforward as in the cases of ground-based observations. Here, we used the more rigorous approach of the "instrument operator" (see equation below), after interpolation of the model profile to the first six levels of the satellite product (Rodgers, 2000):

$$\ln(v^{ret}) = \ln(v^{a}) + A(\ln(v^{true}) - \ln(v^{a})) \qquad Eq.\ 1$$

where v^{ret} is the retrieved profile concentration vector, v^{a} is a priori profile concentration vector, v^{true} is the true profile concentration vector, and A is the averaging kernel matrix in logarithmic space (for each 0.5°×0.5° resolution grid-cell). In our inversion setup, we directly compared the retrieved v^{ret} and the observed satellite column concentration v^{sat} that is given by CrIS. In our case, v^{true} is equal to the modelled concentration v^{mod} calculated from the SRMs and a prior emission inventory. The argument for this approach is that v^{ret} is what the satellite would observe if v^{mod} was the true profile. This is a useful technique for evaluating if the retrieval algorithm is performing as designed, i.e., is it unbiased and the calculated root mean square error (RMSE) is within the expected variability. Further details about the algorithm and the setup can be found in Tichý et al. (2023).

The goal of the inversion is to iteratively update prior emissions by minimizing the distance between v^{sat} and v^{ret} by correcting the emission flux x in the term $v^{mod} = srm^{Flex}x^{a}$ (srm^{Flex} denotes the FLEXPART SRMs), at each grid-cell and each of the six vertical levels that are important for CrIS (Sitwell et al., 2022):

$$\arg\min_{x^{a}\to x} \left|\left|v^{sat} - v^{ret}\right|\right|_{2}^{2} \qquad Eq.\ 2$$

The inverse problem is constructed for each spatial element of the computational domain. Inspired by the construction of covariance matrix in Cao et al. (2020), we consider 4° surroundings (445 km), expressed by the index set $\mathbb{S}$, of which the column concentrations are considered due to computational effectivity. Note that we observed low sensitivity of resulting emission estimates to this choice. Then, we can formulate the inverse problem for each spatial element as:

$$\left[v_{s_i}^{sat};\ s_i \in \mathbb{S}\right] = \left[v_{s_i}^{ret};\ s_i \in \mathbb{S}\right] q^{\mathbb{S}} \qquad Eq.\ 3$$

where the left side of the equation is formed by the vector with aggregated CrIS observations, vectors $v_{s_i}^{ret}$ form a block-diagonal matrix, and $q^{\mathbb{S}}$ is an unknown vector with correction coefficients for each temporal element of the emission. The inverse problem in Eq. 3 was solved using the least squares with adaptive prior covariance (LS-APC) algorithm (Tichý et al., 2016). The algorithm is based on a

Bayesian model which assumes that all coefficients are positive and that the abrupt changes in their neighbouring values are less probable. It is shown that the method is less sensible to manual tunning of regularization parameters (see sensitivity tests in Tichý et al. (2020)) than classical optimization procedures, which is crucial for such a large dataset where each spatial element represents a separate inverse problem.

A detailed description of the algorithm is given in Tichý et al. (2016). Here, we do not describe the algorithm again but explain a few modifications that were necessary for this study. By estimating the correction coefficients $q^{\$}$ for each grid-cell of the spatial domain (10°W–50°E, 25°N–75°N), we can propagate the coefficients through Eq. 2 to update a priori emissions x^a in the model concentration term v^{mod}. We follow Li et al. (2019) and Cao et al. (2020) to bound the ratio between the prior and the posterior emissions. The lower and upper bound of this ratio is set to 0.01 and 100, respectively, to omit the unrealistically low or high emissions. We consider these bounds large enough to allow for new emission sources to be exposed, not presented in the prior emissions.

We evaluate the performance of the inversion by using three a priori emission datasets, (i) one based on Van Damme et al. (2018) calculations (Evangeliou et al., 2021) (hereafter denoted as "VD"), (ii) the ECLIPSEv6 inventory (Klimont, 2022; Klimont et al., 2017) (combined with biomass burning emissions from GFEDv4 (Giglio et al., 2013)) as the most recent one (denoted as "EC6G4"), and (iii) the average of four emission inventories for ammonia, except for these two mentioned before, "EGG" (see previous section), and "NE" calculated from IASI (Infrared Atmospheric Sounding Interferometer) observation (Evangeliou et al., 2021) (denoted as "avgEENV"). To account for the spatiotemporal impact of the lockdown on the European emissions, we corrected prior emission inventories of ammonia (EGG, EC6G4 and avgEENV) for 2020 using adjustment factors (AFs) adopted from Doumbia et al. (2021). The same was done for SO_2 and NO_x (precursors of sulfuric and nitric acid in the atmosphere) in EGG that was used to calculate ammonia's loss rates using LMDz-OR-INCA model (see section 2.2). This dataset provides, for the January–August 2020 period, gridded AFs at a 0.1°×0.1° resolution on a daily resolution for transportation (road, air and ship traffic), power generation, industry and residential sectors. The quantification of AFs is based on activity data collected from different databases and previously published studies. These emission AFs have been applied to the CAMS global inventory, and the changes in emissions of the main pollutants have been assessed for different regions of the world in the first 6 months of 2020 (Doumbia et al., 2021).

Figure *1* shows the comparison of prior and posterior concentrations against independent observations (observations that were not used in the inversion algorithm) from the EMEP network (https://emep.int/mscw/, **Figure S *1***) for January–July 2020. Note that prior concentrations of

ammonia result by coupling the FLEXPART SRMs with prior emissions (from VD, ECLIPSEv6 and avgEENV), while posterior concentrations by coupling the SRMs with the calculated posterior emissions. In **Figure *1*** it is evident that the most accurate reconstruction of surface concentrations with respect to the EMEP observations was obtained using avgEENV as the a priori information, and therefore the results presented hereafter are based on this setup. We performed inversions for the first half of 2020 to assess the effect of lockdown measures on ammonia emissions, as well as the situation after lockdown measures were taken away (rebound period). To have a more generic view, we also performed inverse modelling calculations for the first half of each year between 2016–2019 (reference period). Then, we assess in impact of ammonia changes on aerosol formation (PM2.5), by feeding the posterior emissions to the LMDz-OR-INCA model and calculating the production of PM2.5.

2.4 Statistical tests

To evaluate the comparisons between modelled and observed concentrations of ammonia, we used the root mean squared logarithmic error (RMSLE) defined as follows:

$$RMSE = \sqrt{\sum_{i=1}^{N} \frac{(C_m - C_o)^2}{N}} \quad \text{and} \quad RMSLE = \sqrt{\frac{1}{N}\sum_{i=1}^{N}(\log C_m - \log C_o)^2} \qquad Eq.\ 4$$

where C_m and C_o are the modelled and measured ammonia concentrations and N is the total number of observations. The commonly used squared Pearson correlation coefficient (r) was also used as a measure of linear correlation between two sets of data defined as:

$$r = \frac{\sum(C_m - \overline{C_m})(C_o - \overline{C_o})}{\sqrt{(C_m - \overline{C_m})^2 (C_o - \overline{C_o})^2}} \qquad Eq.\ 5$$

where the distance of modelled and measured ammonia concentrations from the mean ($\overline{C_m}$ and $\overline{C_o}$) is computed. Finally, the standard deviation was adopted as a measure of the dispersion of modelled ammonia from the observations, which is the true value:

$$\sigma = \sqrt{\frac{(C_m - C_o)^2}{N}} \qquad Eq.\ 6$$

The mean fractional bias (MFB) was selected as a symmetric performance indicator that gives equal weights to under- or over-estimated concentrations (minimum to maximum values range from -200% to 200%). It was used in the independent validation (validation against measurements that were excluded from the inversion, see section **3.3**) of the posterior concentrations of ammonia during the European lockdowns of 2020 and is defined as:

$$MFB = \frac{1}{N}\frac{\sum_{i=1}^{N}(C_m - C_o)}{\sum_{i=1}^{N}(\frac{C_m + C_o}{2})} \qquad Eq.\ 7$$

For the same reason, the mean absolute error was computed normalized ($nMAE$) over the average of all the actual values (observations here), which is a widely used simple measure of error:

$$MAE = \frac{\sum_{i=1}^{N}|C_m - C_o|}{\sum_{i=1}^{N} C_o} \qquad Eq.\ 8$$

3 Results

3.1 Emission changes of ammonia due to COVID-19 restrictions over Europe

The reason behind the selected three priors used in the inversion (EGG, EC6G4 and avgEENV) of ammonia is trifold; (i) they are based on the most recent estimates, (ii) they present different spatial distribution, and (iii) they were derived using different methodologies. More specifically, EC6G4 is based on the emission model GAINS (Klimont et al., 2017), while VD uses satellite observations combined with a box model (Evangeliou et al., 2021). As mentioned in the previous section, it is seen that the most accurate representation of surface model concentrations was achieved using the avgEENV a priori, which forces posterior concentrations closer to 1×1 line, whereas the obtained statistics are significantly better than using other priors (**Figure *1***). Therefore, the results presented below have all been obtained using avgEENV as the prior emission dataset keeping results using the other two priors in the Supplements.

The total prior emissions of ammonia over Europe for the inversion period (January – June), the posterior emissions for years 2016–2019 and the posterior emissions during the lockdown year 2020 (January – June) are plotted in **Figure *2*** (the results from inversions using EC6G4 and VD prior emissions are illustrated in **Figure S *2*** and ***S 3***). The total prior ammonia emitted between January and June in Europe were equal to 1061 kt (**Figure *2***a). To check whether calculated changes in 2020 were due to meteorology and avoid misinterpretation of our findings, inverse calculations of ammonia were performed for the reference years 2016–2019 (January–June) using respective observations from CrIS and exactly the same set-up as the one described in section 2 (Methods). The total posterior emissions of ammonia over Europe for the reference period (2016 – 2019) were estimated to be 1665±330 kt (4-y mean±SD) or 57% higher than the prior (**Figure *2***b). Finally, for January–June 2020 the derived emission estimates were equal to 1568±172 kt (posterior±uncertainty) (**Figure *2***c). This is 48% higher than the prior and 6% lower than the posterior emissions of January–June 2016–2019.

The weekly-average evolution of prior and posterior emissions of ammonia over Europe (January to June) for 2016–2019 show a similar pattern with small year-to-year variability (**Figure *2***d,e), and similar temperatures (**Figure S *4***) thus insignificant impact from the prevailing

meteorology that would justify change in emissions due to volatilisation. The weekly posterior ammonia emissions over Europe changed during the lockdown period (2020) as compared to the reference years (**Figure *2***f). Satellites and national monitoring measurements of ammonia show that emissions peak in spring (March) and late-summer in Europe (Van Damme et al., 2022) corresponding to the two main fertilization periods (Paulot et al., 2014). Ammonia abundances are however high throughout the entire spring–summer period due to agriculture associated with rising temperature (Sutton et al., 2013). Ammonia posterior emissions in 2020 declined by -9.8% as compared to the same period over the previous four years (2016–2019, **Figure *2***f). Although the obtained posterior emissions for the reference period (dashed grey line and shade) are very similar to those of 2020, (solid blue line and shade in **Figure *2***f), emissions during lockdown period in 2020 dropped substantially, outside of the deviation of the emissions in the reference period (**Figure *2***f).

3.2 Uncertainty of the posterior emissions

As described in section 2.3 in more detail, we considered 4° surroundings of each spatial element of our inversion domain from which the CrIS observations were used in the inverse problem. This means that 45 spatial elements in CrIS space were used, with six vertical levels each, for each of the 26 temporal emission elements. To calculate the associated uncertainty of the posterior estimates, we tested two sources of uncertainty: (i) how different surroundings for each spatial element affect posterior emissions of ammonia and (ii) how the use of different prior emissions affects posterior ammonia. We organized a series of sensitivity tests using surroundings covering 2°, 3° and 4° from each grid-cell. This selection is realistic as it was shown previously in Cao et al. (2020) for the construction of prior emission error covariance matrix. For the second source of uncertainty, we performed the same inversion using not only EC6G4 and VD priors, but also adding results using two more datasets for ammonia (in total four), which have 10 times higher emissions, namely EGG and NE (see section 2.3).

The calculated absolute uncertainties are depicted in **Figure *3***a–c together with the relative uncertainty (**Figure *3***d) with respect to the posterior emissions of ammonia (posterior ammonia is shown in **Figure *2***c). The first source of uncertainty (different surroundings) slightly affects the resulting posterior emissions of ammonia (**Figure *3***a) causing an average relative uncertainty below 4% in the European emissions. The second source of uncertainty (use of different priors) causes much larger bias as shown in **Figure *3***b (average relative uncertainty 35%). The reason for this is obviously the large variation of the EGG (Bouwman et al., 1997; Giglio et al., 2013; Klimont et al., 2017) and NE (Evangeliou et al., 2021) prior datasets that have total emissions in the first half of 2020 of 63.5 and 53.3 Tg, respectively, in contrast to only 6.2 and 5.7 Tg for EC6G4 and VD. Hence, the results presented here are sensitive to the use of prior emission dataset. The modelled concentrations (that replaces the hypothetical true column concentration in Eq. 1) is calculated by the SRMs and the prior

emission and, therefore, play a key role in the comparison of the CrIS value (v^{sat}) and retrieved value (v^{ret}) (see Eq. 2). Also, the modelled concentrations stand as the argument of the natural logarithm weighted by the averaging kernel in logarithmic space. The linearization of this operator as suggested by Sitwell and Shephard (2021) may reduce the dependency on the prior emission term, however, this is beyond the scope of this study. Overall, the propagated (absolute and relative) uncertainties of the posterior emissions are shown in **Figure *3***c and d and are equal to 11% over Europe on average (**Figure *3***). The latter shows that our calculations are robust on one hand, but dependent on the use of a priori information on the other.

3.3 Validation of posterior ammonia against independent measurements

The optimized emissions of ammonia must be validated against independent observations, because the inversion algorithm has been designed to reduce the model–observation mismatches. Here, the reduction of the posterior concentration differences from the observations from CrIS is determined by the weighting that is given to the observations and, hence, such comparison depends on this weighting (dependent observations). Therefore, the ideal comparison of any posterior emission resulting from top-down methods would be against measurements that were not included in the inversion algorithm (independent observations). Here, we used ground-based observations of ammonia from all EMEP sites (https://emep.int/mscw/) for the period of our study as an independent dataset for validation. All stations are illustrated in **Figure S *1***.

As we mentioned in section 2.3, we evaluated the efficiency of the inversion and the most effective a priori dataset for our purpose by assessing the match between the calculated posterior concentrations against all the available observations from EMEP (N=3957) for the study period (**Figure *1***). More specifically, after it became evident that the most accurate results were obtained with avgEENV as the prior (relationship closer to unity against measured ammonia), we saw an immediate improvement in the statistical tests used (nRMSE, nMAE and RMSLE) when using the posterior emissions to model ammonia in FLEXPART during the first half of 2020 (**Figure *1*** – right panel). nMAE decreased from 0.80 using the prior emissions to 0.76 using the posterior ones, accordingly nRMSE of the posterior concentrations dropped to 0.073 as compared to -0.069 using the prior emissions, while the RMSLE decreased from 0.60 using prior emissions to 0.55 using the optimized a posteriori emissions. To get a better insight on how modelled concentrations improved towards ammonia observations, eight random EMEP stations were selected to show timeseries of prior and posterior concentrations in the first half of 2020 (**Figure S *5***). Although large peaks were not reproduced, all statistics were improved using the posterior emissions of ammonia.

3.4 Country-level changes due to COVID-19 restrictions

To document the emission changes of ammonia over the different European countries before, during and after the 2020 lockdowns, we report the weekly evolution of the emissions for 16 countries individually (**Figure *4***). Specifically, weekly emissions were averaged for each country based on respective country definitions that are shown in **Figure S *6*** using the avgEENV prior.

Most countries show that ammonia emissions declined or at least stayed less affected by the 2020 lockdowns, as compared to the same period during the reference years (2016–2019). Countries with substantial decreases in the 2020 lockdown emissions were The Netherlands (-16%) and Belgium (-23%), both countries with important agricultural activity, as well as Denmark (-20%), Ireland (-18%) and Ukraine (-18%). Smaller changes were recorded in Spain (-2.1%), Czechia (-4.0%) and Italy (-6.0%) despite the intensive lockdown measures. This practically shows that agricultural activity is insignificantly affected, even in periods of extraordinary austerity, as the last remaining primary production sector, necessary for human life.

We note that the largest emissions of ammonia in European countries were seen around March–April (weeks 8–16) and in summer. These coincide with the fertilization periods mentioned previously (Paulot et al., 2014) that control the seasonality of ammonia's emissions. In most European countries, the time of the year when fertilizers can be applied is tightly regulated (Ge et al., 2020). In the Netherlands and Belgium, for instance, the largest ammonia contributing region in Europe, application of nitrogen fertilizer is only allowed from February to mid-September. This produces two peak periods, in March and late May (**Figure *4***). Manure application also follows stringent regulations and is only allowed in the same periods depending on the type of manure (slurry or solid) and the type of land (grassland or arable land) (Van Damme et al., 2022).

To understand and position where ammonia emissions changed during the European lockdowns of 2020, we plot the difference of the posterior emissions of ammonia during the lockdown period (15 March – 30 April) for the same period in **Figure *5***a. We calculate higher emissions of ammonia during the lockdown of +115 kt as compared to the prior emissions. Note that inversion algorithms aim at reducing the mismatches between modelled concentrations and observations (in our case, from CrIS satellite measurements) by correcting emissions. This means that different posterior emissions are most likely, due to errors in the prior emissions and do not indicate any impact from the restriction measures.

Therefore, we demonstrate the impact of the COVID-19 lockdowns over Europe in 2020, by calculating the emission anomaly for the lockdown period from 2016–2020 (same period as the 2020 lockdowns, namely 15 March – 30 April) in **Figure *5***b. Emissions during the 2020 lockdowns

dropped by -29 kt with respect to the same period in 2016 – 2020 showing the impact of the COVID-19 restrictions. Maximum decreases were seen in The Netherlands and Belgium, both countries comprising high emissions (**Figure *5***b) that also suffered heavily from the COVID-19 outbreak (Bendz and Aaberge, 2020) and took strict lockdown measures. Other areas where significant changes were calculated were Northern Italy, Switzerland and Austria, while Scandinavian countries were not affected. This agrees well with the state of the epidemic in these countries in spring 2020. While North Italy was the first country outside China to suffer high mortality rates and, thus, dramatic social restrictions in spring 2020, Norway, Sweden, Denmark and Finland showed total infected cases far below 1% per capita, mostly suffering higher rates later in 2020 (Gordon et al., 2021).

As mentioned previously, ammonia emissions increase in spring (March) and late-summer in Europe (Van Damme et al., 2022; Paulot et al., 2014). Therefore, calculating the difference in the calculated emissions during the lockdown from the period before or after is practically meaningless and cannot show the lockdown impact since agricultural activity was slightly affected in 2020. For this reason we quantify the delay in the evolution of the 2020 emissions by calculating emission differences in the lockdowns from the period before (Lock – Prelock) for the lockdown year 2020 and emission differences (Lock – Prelock) for the reference years (2016 – 2019). Then, we plot their spatial differences in **Figure *5***c. Accordingly, we do the same calculation for differences in the rebound period (the period after the restrictions were relaxed) from the lockdown period (Rebound – Lock) in 2020 and compare them with Rebound – Lock for the reference years 2016 – 2019 (**Figure *5***d). We observe a clear delay in the evolution of ammonia emissions in 2020 of -77 kt (**Figure *5***c), while only Scandinavian countries show positive changes. Hot-spots of negative evolution were seen in central Europe, mainly in the triptych of Northern Italy, Switzerland and Austria, for the reasons discussed in the previous paragraph. In Poland, social measures affected the daily lives of citizens significantly (Szczepańska and Pietrzyka, 2021) and might be the reason for the decreased evolution of ammonia emissions (**Figure *5***c). After the measures were relaxed, the evolution of the emissions rebounded slightly with respect to the reference period (2016 – 2019) as shown in **Figure *5***d. The changes in ammonia during the rebound period were concentrated in countries that were affected most severely from the lockdown restrictions, namely Northern Italy, Switzerland, Austria and Poland. The same has been reported elsewhere for several other pollutant emissions (Davis et al., 2022; Jackson et al., 2022).

4 Discussion

4.1 Rising ammonia concentrations during the European lockdowns

One issue that has been overlooked is the concentrations of ammonia before, during and after the 2020 lockdowns in Europe. Despite the delay in the emissions during the lockdown period in 2020 (section 3.4), satellite ammonia from CrIS showed an increase during the lockdowns and declined after the restrictions were relaxed in almost all European countries (**Figure *4***). The latter was reported in several studies analysing ground-based measurements. For example, Lovarelli et al. (2021) concluded that contrary to other air pollutants, ammonia was not reduced, when the COVID-19 restrictions were introduced in North Italy. They further reported that urban and rural ammonia was the highest compared to previous years during the same months for which the strictest lockdowns occurred (i.e., spring 2020). Rennie et al. (2020) reported a slight decrease of ammonia in the UK, while Xu et al. (2022) observed increased of ambient ammonia during the lockdowns in China. Accordingly, Viatte et al. (2021) found enhanced ammonia during lockdown in Paris. Finally, in a recent study, Kuttippurath et al. (2023) reported increase in ammonia during lockdowns almost everywhere, with maxima in Western Europe, Eastern China, the Indian subcontinent and the Eastern USA. Since atmospheric ammonia has been increasing globally due to various anthropogenic activities, the European lockdowns in 2020 offer a unique opportunity to expose ammonia's sources and address the importance of secondary PM2.5 formation.

Figure *6*a depicts the modelled atmospheric lifetime of ammonia and its dependence from the calculated loss-rates over Europe for the first half of 2020. Ammonia is a particularly interesting substance due to its affinity to react with atmospheric sulfuric and nitric acids producing secondary aerosols. However, the reaction with sulfuric acid is more prevalent due to several factors. For instance, sulfuric acid is a stronger acid than nitric acid, leading to more efficient reactions with ammonia (higher reaction rate constant for ammonia with sulfuric than with nitric acid, thus faster formation of ammonium sulfate) (Behera and Sharma, 2012). Furthermore, ammonium sulfate (final product of ammonia reaction with sulfuric acid) is less volatile and more thermodynamically stable than ammonium nitrate (product of the reaction with nitric acid) favoring the formation and persistence of ammonium sulfate particles in the atmosphere (Walters et al., 2019). Finally, sulfuric acid forms more stable clusters with ammonia, even in the presence of nitric acid (Liu et al., 2018). Results from laboratory and field studies have confirmed that ammonia actually promotes the nucleation of sulfuric acid in the atmosphere (Weber et al., 1999; Schobesberger et al., 2015). The CLOUD (Cosmics Leaving Outdoor Droplets) experiment has also highlighted that ammonia preferentially reacts with sulfuric acid in the atmosphere due to its strong acidity, ability to drive stable aerosol formation, and significant nucleation enhancement effects (Kirkby et al., 2016; Wang

et al., 2022). Nitric acid plays a secondary role, primarily forming ammonium nitrate once sulfuric acid has reacted, but its contribution is limited by its volatility.

During the lockdown period over Europe, transport and industrial activities mostly stopped, and consequently the related emissions also decreased. This had an immediate effect on SO_2 and NO_x (Guevara et al., 2021; Doumbia et al., 2021). Reductions of SO_2 and NO_x caused less production of atmospheric sulfuric and nitric acids. The latter had a rapid twofold effect on the lifetime of ammonia: (i) Less available atmospheric acids needed less ammonia for reaction towards sulfate (mainly) and nitrate aerosols (secondarily) and therefore the loss-rates declined (**Figure *6***a) leading to accumulation of ammonia in its free form; (ii) ammonia originates mainly from agriculture and livestock, and these activities were slightly affected during the European lockdowns increasing the associated emissions (see **Figure *2***, though with a lower trend than previous years as discussed in section 3.4). The rising levels of ammonia during the COVID-19 lockdowns in Europe have been confirmed by the CrIS observations (**Figure *2*** and ***3***) and have been also reported elsewhere (Kuttippurath et al., 2023; Viatte et al., 2021; Xu et al., 2022; Lovarelli et al., 2021).

4.2 Disturbance in the secondary formation of PM2.5

The response of the restriction measures on PM2.5 mass concentrations suggests a relationship that is more complex than expected and beyond road traffic intensity, at least for Europe. It has been reported that there was no systematic decrease in PM2.5 concentrations during COVID-19 lockdowns in the USA (Archer et al., 2020; Bekbulat et al., 2021) or even in Chinese cities (Mo et al., 2021), where primary sources are abundant and stringent lockdown measures decreased PM levels (Zhang et al., 2023). In a recent study focusing on PM2.5 measurements over 30 urban and regional background European sites, Putaud et al. (2023) showed that the implementation of the lockdown measures resulted in minor increases in PM2.5 mass concentration in Europe of +5±33%. The latter aligns well with several regional studies focusing on the impact of lockdowns to regional pollution (Querol et al., 2021; Shi et al., 2021; Viatte et al., 2021; Thunis et al., 2021; Putaud et al., 2021).

Figure *6*b demonstrates observed PM2.5 from the EMEP stations (78 sites) in comparison with modelled PM2.5 concentrations, both averaged for all sites. In modelled PM2.5 mass concentrations, we have separated primary and secondary PM2.5, as secondary PM2.5 is modulated by the chemical state of the atmosphere as defined by the abundance in acids and free ammonia. We see that observed and modelled PM2.5 concentrations are in good agreement in the first half of 2020. The good agreement between modelled and observed concentrations can be also confirmed for most of the EMEP stations over Europe with high Pearson's coefficients, low RMSE's and low standard deviations in the Taylor plot that is demonstrated in **Figure S 7**. Furthermore, while secondary PM2.5 constitute around 20-30% of the total PM2.5 (Dat et al., 2024; Bressi et al., 2013; Li et al., 2023), this

proportion increased during the European lockdowns despite that reactions of ammonia to form PM2.5 were decelerated (as seen by the declined loss in **Figure *6***a).

Leung et al. (2020) reported that the abatement of nitrate in China is buffered not only by increased oxidant build-up, but also by an increase in free ammonia concentrations through sulfate concentration reduction, which favours ammonium nitrate formation. During COVID-19 restrictions in Europe, a significant decrease of NO_x (and SO_2) emissions occurred (Guevara et al., 2021) also confirmed by Doumbia et al. (2021). Thunis et al. (2021) showed that the latter might have increased the oxidative capacity of the atmosphere and, in turn, PM2.5 formation. This is the main reason why PM2.5 concentrations were not decreased during the COVID-19 lockdowns in many European cities (Varotsos et al., 2021; Shi et al., 2021), while the same has been reported elsewhere (Huang et al., 2021; Le et al., 2020; Zhang et al., 2022).

PM2.5 increased at areas less affected by primary emissions during the 2020 lockdown or at areas where the oxidative atmosphere favours secondary aerosol formation. For instance, reductions in PM2.5 were observed to be less pronounced than those in nitrogen dioxide in several regions (Patel et al., 2020; Shi and Brasseur, 2020), while PM2.5 even increased in others (Wang et al., 2020; Li et al., 2020). Li et al. (2020) indicated that while primary emissions dropped by 15–61% in China, daily average PM2.5 concentrations were still very high (15–79 μg m-3) showing that background and residual pollutants were important. In a similar manner, an extreme PM2.5 pollution event during the Chinese lockdown in Nanning that cause public concern was due to secondary aerosol formation (Mo et al., 2021).

Here we aim at interpreting the mechanism below this disturbance in PM2.5 formation. As explained in Seinfeld and Pandis (2000) and represented in the LMDZ-INCA model (Hauglustaine et al., 2014), the neutralisation of atmospheric acids by ammonia in the atmosphere occurs through ammonium sulfate formation. Sulfate ($SO_{4\,(s)}^{2-}$) is also produced from sulfur dioxide ($SO_{2\,(g)}$) gas phase oxidation by the hydroxyl radical (OH). Note that the hydroxyl radical is mostly formed in the atmosphere when ultraviolet radiation (UV) photolyses ozone in the presence of water vapour, hence it is linked to humidity (**Figure S *8***). Sulfate production can also occur in the aqueous phase (Hoyle et al., 2016) through sulfur dioxide ($SO_{2\,(aq)}$) oxidation with ozone ($O_{3\,(aq)}$) or hydrogen peroxide ($H_2O_{2\,(aq)}$). In both phases, a higher humidity favors sulfate formation (**Figure S *8***). Ammonia also reacts with nitric acid ($HNO_{3\,(g)}$) to form ammonium nitrate ($NO_{3\,(s)}^{-}$) in an equilibrium reaction. In that case, as SO_2 is strongly decreased due to the restrictions (Doumbia et al., 2021) and more free ammonia accumulates (see previous section), these higher gaseous ammonia levels increase the particulate nitrate formation. This mechanism has been highlighted in China as an unintended consequence of the of NO_x and SO_2 regulation on the PM2.5 levels (Lachatre et al., 2019).

Conducting specific experiment in the frame of the CLOUD collaboration, Wang et al. (2022) reported that the NH_3 - H_2SO_4 - HNO_3 system forms particles synergistically, at rates orders of magnitude faster than those the individual reactions of ammonia with sulfuric or nitric acid can give. In addition to this mechanism, as the fraction of the total inorganic nitrate, as particulate $NO_{3\,(s)}^-$ (instead of gaseous $HNO_{3\,(g)}$), increases, and as NO_x and SO_2 decrease, while NH_3 emissions remain high, a small increase in the particulate fraction greatly slows down deposition of total inorganic $NO_{3\,(s)}^-$ and hence drives particulate $NO_{3\,(s)}^-$ to increase (Zhai et al., 2021). Thus, although NO_x emissions decreased during COVID-19 lockdowns in Europe, secondary PM2.5 stayed unchanged, because NO_x emissions reduction drives faster oxidation of NO_x and slower deposition of total inorganic $NO_{3\,(s)}^-$.

5 Conclusion

We have examined the impact of lockdown measures in Europe due to COVID-19 on the atmospheric levels and emissions of ammonia using high-resolution satellite observations combined with a dispersion model and an inverse modelling algorithm. We find that ammonia emissions in 2020 declined by -9.8% as compared to the same period in previous years (2016–2019). However, this decrease is insensitive to the meteorological conditions, as the 2020 ammonia emissions during the European lockdowns dropped outside of the deviation of the emissions in the reference period (2016–2019), while temperature, humidity and precipitation showed limited variability.

While ammonia emissions generally increase in spring and late summer in Europe due to fertilisation, during the 2020 lockdowns, a clear delay in the evolution of the emissions of -77 kt was calculated, mostly in the central European countries, which suffered by the stringent restrictions. The evolution of ammonia emissions slightly rebounded after the restrictions were relaxed.

During the COVID-19 lockdowns of 2020 over Europe the atmospheric levels of ammonia were drastically increased, as confirmed by ground-based and satellite observations. The reason for this is twofold; first, the European lockdown measures reduced atmospheric emissions and levels of SO_2 and NO_x and their acidic products (H_2SO_4 and HNO_3) slowing down binding and chemical removal of ammonia (lifetimes increased), and thus accumulating free ammonia; second, the prevail of agricultural activity during the lockdowns increased ammonia emissions (though at a lower rate).

Surprisingly, despite all the travel, working and social restrictions that the European governments took to combat the outbreak of COVID-19, ambient pollution levels did not change as expected. PM2.5 levels were modulated by the chemical state of the atmosphere through secondary aerosol formation. Secondary PM2.5 rather increased during the European lockdowns despite that the

precursors of H_2SO_4 and HNO_3 declined. More sulfate was produced from SO_2 and OH (gas phase) or O_3 (aqueous phase), while both atmospheric reactions were favoured by higher water vapour (humidity) during the lockdown period. The accumulated ammonia reacted with H_2SO_4 first producing sulfate. Then, as SO_2 decreased during the European lockdowns and more free ammonia accumulated, the high excess gaseous ammonia reacted with HNO_3 shifting the equilibrium reaction towards conversion to particulate nitrate causing unintended increase in the PM2.5 levels. While NO_x emissions declined during the European lockdowns by -33%, this reduction drives faster oxidation of NO_x and slower deposition of total inorganic nitrate causing high secondary PM2.5 levels.

The present study gives a comprehensive analysis of the atmospheric NH_3 - H_2SO_4 - HNO_3 system. It also proves the complicated relationship of secondary PM2.5 formation with the abundant atmospheric gases. The general drop of emissions during the first consistent lockdowns of 2020 in Europe offers a unique opportunity to study atmospheric chemistry under extreme conditions of fast pollutant emission drop equivalent to "The Clean Air Action" of the Chinese government.

Data availability. All data from this study are available for download from https://datadryad.org/stash/share/Wgbc9UiXwtMH44366myWh2bt7MQc92JKhJBz7UwQlgY (reserved doi: 10.5061/dryad.12jm63z1q). The EMEP measurements of ammonia can be downloaded from https://ebas.nilu.no. The remote sensing data for ammonia can be retrieved from https://hpfx.collab.science.gc.ca/~mas001/satellite_ext/cris/snpp/nh3/v1_6_4/ or upon request to Dr. M. W. Shephard. FLEXPART version 10.4 model can be downloaded from https://www.flexpart.eu/downloads.

Supplement. The supplement related to this article in available online at.

Author contributions. NE led the overall study, analysed the results and wrote the paper. OT developed the inverse modelling algorithm and performed the inversions. MSO processed CrIS ammonia on a grid. SE developed FLEXPART version 10.4 model to account for the loss of ammonia from the chemistry transport model LMDz-OR-INCA. YB and DH set up and ran the chemistry transport model LMDz-OR-INCA. All authors contributed to the final version of the manuscript.

Competing interests. The authors declare no competing interests.

Financial support. The work was supported by the COMBAT (Quantification of Global Ammonia Sources constrained by a Bayesian Inversion Technique) project funded by ROMFORSK – Program

for romforskning of the Research Council of Norway (Project ID: 275407, website: https://prosjektbanken.forskningsradet.no/project/FORISS/275407?Kilde=FORISS&distribution=Ar&chart=bar&calcType=funding&Sprak=no&sortBy=date&sortOrder=desc&resultCount=30&offset=0&ProgAkt.3=ROMFORSK-Program+for+romforskning). Dr. Ondřej Tichý was supported by the Czech Science Foundation, grant no. GA24-10400S.

References

Abbatt, J. P. D., Benz, S., Cziczo, D. J., Kanji, Z., Lohmann, U., and Mohler, O.: Solid Ammonium Sulfate Aerosols as Ice Nuclei: A Pathway for Cirrus Cloud Formation, Science (80-.)., 313, 1770–1773, 2006.

Acharya, P., Barik, G., Gayen, B. K., Bar, S., Maiti, A., Sarkar, A., Ghosh, S., De, S. K., and Sreekesh, S.: Revisiting the levels of Aerosol Optical Depth in south-southeast Asia, Europe and USA amid the COVID-19 pandemic using satellite observations, Environ. Res., 193, 110514, https://doi.org/10.1016/j.envres.2020.110514, 2021.

Anderson, N., Strader, R., and Davidson, C.: Airborne reduced nitrogen: Ammonia emissions from agriculture and other sources, Environ. Int., 29, 277–286, https://doi.org/10.1016/S0160-4120(02)00186-1, 2003.

Archer, C. L., Cervone, G., Golbazi, M., Al Fahel, N., and Hultquist, C.: Changes in air quality and human mobility in the USA during the COVID-19 pandemic, Bull. Atmos. Sci. Technol., 1, 491–514, https://doi.org/10.1007/s42865-020-00019-0, 2020.

Baekgaard, M., Christensen, J., Madsen, J. K., and Mikkelsen, K. S.: Rallying around the flag in times of COVID-19: Societal lockdown and trust in democratic institutions, J. Behav. Public Adm., 3, 1–12, https://doi.org/10.30636/jbpa.32.172, 2020.

Bauwens, M., Compernolle, S., Stavrakou, T., Müller, J. F., van Gent, J., Eskes, H., Levelt, P. F., van der A, R., Veefkind, J. P., Vlietinck, J., Yu, H., and Zehner, C.: Impact of Coronavirus Outbreak on NO2 Pollution Assessed Using TROPOMI and OMI Observations, Geophys. Res. Lett., 47, 1–9, https://doi.org/10.1029/2020GL087978, 2020.

Behera, S. N. and Sharma, M.: Transformation of atmospheric ammonia and acid gases into components of PM2.5: An environmental chamber study, Environ. Sci. Pollut. Res., 19, 1187–1197, https://doi.org/10.1007/s11356-011-0635-9, 2012.

Bekbulat, B., Apte, J. S., Millet, D. B., Robinson, A. L., Wells, K. C., Presto, A. A., and Marshall, J. D.: Changes in criteria air pollution levels in the US before, during, and after Covid-19 stay-at-home orders: Evidence from regulatory monitors, Sci. Total Environ., 769, 144693, https://doi.org/10.1016/j.scitotenv.2020.144693, 2021.

Bellouin, N., Rae, J., Jones, A., Johnson, C., Haywood, J., and Boucher, O.: Aerosol forcing in the

639 Climate Model Intercomparison Project (CMIP5) simulations by HadGEM2-ES and the role of
640 ammonium nitrate, J. Geophys. Res. Atmos., 116, 1–25, https://doi.org/10.1029/2011JD016074,
641 2011.
642 Bendz, B. and Aaberge, L.: COVID-19 spread in the UK: the end of the beginning?, Lancet, 396,
643 587–590, https://doi.org/https://doi.org/10.1016/ S0140-6736(20)31689-5 www.thelancet.com,
644 2020.
645 Bouwman, A. F., Lee, D. S., Asman, W. A. H., Dentener, F. J., Van Der Hoek, K. W., and Olivier,
646 J. G. J.: A global high-resolution emission inventory for ammonia, Global Biogeochem. Cycles, 11,
647 561–587, https://doi.org/10.1029/97GB02266, 1997.
648 Bressi, M., Sciare, J., Ghersi, V., Bonnaire, N., Nicolas, J. B., Petit, J. E., Moukhtar, S., Rosso, A.,
649 Mihalopoulos, N., and Féron, A.: A one-year comprehensive chemical characterisation of fine
650 aerosol (PM2.5) at urban, suburban and rural background sites in the region of Paris (France),
651 Atmos. Chem. Phys., 13, 7825–7844, https://doi.org/10.5194/acp-13-7825-2013, 2013.
652 Camargo, J. A. and Alonso, Á.: Ecological and toxicological effects of inorganic nitrogen pollution
653 in aquatic ecosystems: A global assessment, Environ. Int., 32, 831–849,
654 https://doi.org/10.1016/j.envint.2006.05.002, 2006.
655 Cao, H., Henze, D. K., Shephard, M. W., Dammers, E., Cady-Pereira, K., Alvarado, M., Lonsdale,
656 C., Luo, G., Yu, F., Zhu, L., Danielson, C. G., and Edgerton, E. S.: Inverse modeling of NH3
657 sources using CrIS remote sensing measurements, Environ. Res. Lett., 15, 104082,
658 https://doi.org/10.1088/1748-9326/abb5cc, 2020.
659 Cassiani, M., Stohl, A., and Brioude, J.: Lagrangian Stochastic Modelling of Dispersion in the
660 Convective Boundary Layer with Skewed Turbulence Conditions and a Vertical Density Gradient:
661 Formulation and Implementation in the FLEXPART Model, Boundary-Layer Meteorol., 154, 367–
662 390, https://doi.org/10.1007/s10546-014-9976-5, 2015.
663 Chakraborty, I. and Maity, P.: COVID-19 outbreak: Migration, effects on society, global
664 environment and prevention, Sci. Total Environ., 728, 138882,
665 https://doi.org/10.1016/j.scitotenv.2020.138882, 2020.
666 Chen, S., Perathoner, S., Ampelli, C., and Centi, G.: Chapter 2 - Electrochemical Dinitrogen
667 Activation: To Find a Sustainable Way to Produce Ammonia, in: Horizons in Sustainable Industrial
668 Chemistry and Catalysis, vol. 178, edited by: Albonetti, S., Perathoner, S., and Quadrelli, E. A. B.
669 T.-S. in S. S. and C., Elsevier, 31–46, https://doi.org/https://doi.org/10.1016/B978-0-444-64127-
670 4.00002-1, 2019.
671 Cohen, A. J., Brauer, M., Burnett, R., Anderson, H. R., Frostad, J., Estep, K., Balakrishnan, K.,
672 Brunekreef, B., Dandona, L., Dandona, R., Feigin, V., Freedman, G., Hubbell, B., Jobling, A., Kan,
673 H., Knibbs, L., Liu, Y., Martin, R., Morawska, L., Pope, C. A., Shin, H., Straif, K., Shaddick, G.,

Thomas, M., van Dingenen, R., van Donkelaar, A., Vos, T., Murray, C. J. L., and Forouzanfar, M. H.: Estimates and 25-year trends of the global burden of disease attributable to ambient air pollution: an analysis of data from the Global Burden of Diseases Study 2015, Lancet, 389, 1907–1918, https://doi.org/10.1016/S0140-6736(17)30505-6, 2017.

Croft, B., Pierce, J. R., and Martin, R. V.: Interpreting aerosol lifetimes using the GEOS-Chem model and constraints from radionuclide measurements, Atmos. Chem. Phys., 14, 4313–4325, https://doi.org/10.5194/acp-14-4313-2014, 2014.

Van Damme, M., Clarisse, L., Whitburn, S., Hadji-Lazaro, J., Hurtmans, D., Clerbaux, C., and Coheur, P. F.: Industrial and agricultural ammonia point sources exposed, Nature, 564, 99–103, https://doi.org/10.1038/s41586-018-0747-1, 2018.

Van Damme, M., Clarisse, L., Franco, B., Sutton, M. A., Erisman, J. W., Wichink Kruit, R., Van Zanten, M., Whitburn, S., Hadji-Lazaro, J., Hurtmans, D., Clerbaux, C., and Coheur, P. F. ois: Global, regional and national trends of atmospheric ammonia derived from a decadal (2008-2018) satellite record, Environ. Res. Lett., 16, https://doi.org/10.1088/1748-9326/abd5e0, 2021.

Van Damme, M., Clarisse, L., Stavrakou, T., Wichink Kruit, R., Sellekaerts, L., Viatte, C., Clerbaux, C., and Coheur, P. F.: On the weekly cycle of atmospheric ammonia over European agricultural hotspots, Sci. Rep., 12, 1–9, https://doi.org/10.1038/s41598-022-15836-w, 2022.

Dammers, E., Shephard, M. W., Palm, M., Cady-pereira, K., Capps, S., Lutsch, E., Strong, K., Hannigan, J. W., Ortega, I., Toon, G. C., Stremme, W., and Grutter, M.: Validation of the CrIS fast physical NH 3 retrieval with ground-based FTIR, Atmos. Meas. Tech., 87, 2645–2667, 2017.

Dat, N. Q., Ly, B. T., Nghiem, T. D., Nguyen, T. T. H., Sekiguchi, K., Huyen, T. T., Vinh, T. H., and Tien, L. Q.: Influence of Secondary Inorganic Aerosol on the Concentrations of PM2.5 and PM0.1 during Air Pollution Episodes in Hanoi, Vietnam, Aerosol Air Qual. Res., 24, https://doi.org/10.4209/aaqr.220446, 2024.

Davis, S. J., Liu, Z., Deng, Z., Zhu, B., Ke, P., Sun, T., Guo, R., Hong, C., Zheng, B., Wang, Y., Boucher, O., Gentine, P., and Ciais, P.: Emissions rebound from the COVID-19 pandemic, Nat. Clim. Chang., 12, 410–417, https://doi.org/10.1038/s41558-022-01351-3, 2022.

Diffenbaugh, N. S., Field, C. B., Appel, E. A., Azevedo, I. L., Baldocchi, D. D., Burke, M., Burney, J. A., Ciais, P., Davis, S. J., Fiore, A. M., Fletcher, S. M., Hertel, T. W., Horton, D. E., Hsiang, S. M., Jackson, R. B., Jin, X., Levi, M., Lobell, D. B., McKinley, G. A., Moore, F. C., Montgomery, A., Nadeau, K. C., Pataki, D. E., Randerson, J. T., Reichstein, M., Schnell, J. L., Seneviratne, S. I., Singh, D., Steiner, A. L., and Wong-Parodi, G.: The COVID-19 lockdowns: a window into the Earth System, Nat. Rev. Earth Environ., 1–12, https://doi.org/10.1038/s43017-020-0079-1, 2020.

Doumbia, T., Granier, C., Elguindi, N., Bouarar, I., Darras, S., Brasseur, G., Gaubert, B., Liu, Y., Shi, X., Stavrakou, T., Tilmes, S., Lacey, F., Deroubaix, A., and Wang, T.: Changes in global air

pollutant emissions during the COVID-19 pandemic: A dataset for atmospheric modeling, Earth Syst. Sci. Data, 13, 4191–4206, https://doi.org/10.5194/essd-13-4191-2021, 2021.

Dutheil, F., Baker, J. S., and Navel, V.: COVID-19 as a factor influencing air pollution?, Environ. Pollut., 263, 2019–2021, https://doi.org/10.1016/j.envpol.2020.114466, 2020.

Emanuel, K. A.: A Scheme for Representing Cumulus Convection in Large-Scale Models, J. Atmos. Sci., 48, 2313–2329, https://doi.org/10.1175/1520-0469(1991)048<2313:ASFRCC>2.0.CO;2, 1991.

Erisman, J. W., Bleeker, A., Galloway, J., and Sutton, M. S.: Reduced nitrogen in ecology and the environment, Environ. Pollut., 150, 140–149, https://doi.org/10.1016/j.envpol.2007.06.033, 2007.

Erisman, J. W., Sutton, M. a., Galloway, J., Klimont, Z., and Winiwarter, W.: How a century of ammonia synthesis changed the world, Nat. Geosci., 1, 636–639, https://doi.org/10.1038/ngeo325, 2008.

Evangeliou, N., Platt, S., Eckhardt, S., Lund Myhre, C., Laj, P., Alados-Arboledas, L., Backman, J., Brem, B., Fiebig, M., Flentje, H., Marinoni, A., Pandolfi, M., Yus-Dìez, J., Prats, N., Putaud, J., Sellegri, K., Sorribas, M., Eleftheriadis, K., Vratolis, S., Wiedensohler, A., and Stohl, A.: Changes in black carbon emissions over Europe due to COVID-19 lockdowns, Atmos. Chem. Phys., 1–33, https://doi.org/10.5194/acp-2020-1005, 2020.

Evangeliou, N., Balkanski, Y., Eckhardt, S., Cozic, A., Van Damme, M., Coheur, P.-F., Clarisse, L., Shephard, M., Cady-Pereira, K., and Hauglustaine, D.: 10–Year Satellite–Constrained Fluxes of Ammonia Improve Performance of Chemistry Transport Models, Atmos. Chem. Phys., 21, 4431–4451, https://doi.org/10.5194/acp-21-4431-2021, 2021.

Folberth, G. A., Hauglustaine, D. A., Lathière, J., and Brocheton, F.: Interactive chemistry in the Laboratoire de Météorologie Dynamique general circulation model: model description and impact analysis of biogenic hydrocarbons on tropospheric chemistry, Atmos. Chem. Phys., 6, 2273–2319, https://doi.org/10.5194/acp-6-2273-2006, 2006.

Forster, C., Stohl, A., and Seibert, P.: Parameterization of convective transport in a Lagrangian particle dispersion model and its evaluation, J. Appl. Meteorol. Climatol., 46, 403–422, https://doi.org/10.1175/JAM2470.1, 2007.

Fowler, D., Muller, J. B. A., Smith, R. I., Dragosits, U., Skiba, U., Sutton, M. A., and Brimblecombe, P.: A CHRONOLOGY OF NITROGEN DEPOSITION IN THE UK, Water, Air, Soil Pollut. Focus, 4, 9–23, 2004.

Ge, X., Schaap, M., Kranenburg, R., Segers, A., Jan Reinds, G., Kros, H., and De Vries, W.: Modeling atmospheric ammonia using agricultural emissions with improved spatial variability and temporal dynamics, Atmos. Chem. Phys., 20, 16055–16087, https://doi.org/10.5194/acp-20-16055-2020, 2020.

744 Giani, P., Castruccio, S., Anav, A., Howard, D., Hu, W., and Crippa, P.: Short-term and long-term
745 health impacts of air pollution reductions from COVID-19 lockdowns in China and Europe: a
746 modelling study, Lancet Planet. Heal., 4, e474–e482, https://doi.org/10.1016/S2542-
747 5196(20)30224-2, 2020.
748 Giglio, L., Randerson, J. T., and van der Werf, G. R.: Analysis of daily, monthly, and annual burned
749 area using the fourth-generation global fire emissions database (GFED4), J. Geophys. Res.
750 Biogeosciences, 118, 317–328, https://doi.org/10.1002/jgrg.20042, 2013, 2013.
751 Gordon, D. V., Grafton, R. Q., and Steinshamn, S. I.: Cross-country effects and policy responses to
752 COVID-19 in 2020: The Nordic countries, Econ. Anal. Policy, 71, 198–210,
753 https://doi.org/10.1016/j.eap.2021.04.015, 2021.
754 Gu, B., Sutton, M. A., Chang, S. X., Ge, Y., and Chang, J.: Agricultural ammonia emissions
755 contribute to China's urban air pollution, Front. Ecol. Environ., 12, 265–266,
756 https://doi.org/10.1890/14.WB.007, 2014.
757 Guevara, M., Jorba, O., Soret, A., Petetin, H., Bowdalo, D., Serradell, K., Tena, C., Van Der Gon,
758 H. D., Kuenen, J., Peuch, V. H., and Pérez Garciá-Pando, C.: Time-resolved emission reductions for
759 atmospheric chemistry modelling in Europe during the COVID-19 lockdowns, Atmos. Chem.
760 Phys., 21, 773–797, https://doi.org/10.5194/acp-21-773-2021, 2021.
761 Hauglustaine, D. A., Hourdin, F., Jourdain, L., Filiberti, M.-A., Walters, S., Lamarque, J.-F., and
762 Holland, E. A.: Interactive chemistry in the Laboratoire de Meteorologie Dynamique general
763 circulation model: Description and background tropospheric chemistry evaluation, J. Geophys.
764 Res., 109, https://doi.org/10.1029/2003JD003957, 2004.
765 Hauglustaine, D. A., Balkanski, Y., and Schulz, M.: A global model simulation of present and
766 future nitrate aerosols and their direct radiative forcing of climate, Atmos. Chem. Phys., 14, 11031–
767 11063, https://doi.org/10.5194/acp-14-11031-2014, 2014.
768 Heald, C. L., Collett, J. L., Lee, T., Benedict, K. B., Schwandner, F. M., Li, Y., Clarisse, L.,
769 Hurtmans, D. R., Van Damme, M., Clerbaux, C., Coheur, P. F., Philip, S., Martin, R. V., and Pye,
770 H. O. T.: Atmospheric ammonia and particulate inorganic nitrogen over the United States, Atmos.
771 Chem. Phys., 12, 10295–10312, https://doi.org/10.5194/acp-12-10295-2012, 2012.
772 Henze, D. K., Shindell, D. T., Akhtar, F., Spurr, R. J. D., Pinder, R. W., Loughlin, D., Kopacz, M.,
773 Singh, K., and Shim, C.: Spatially Refined Aerosol Direct Radiative Forcing Efficiencies, Environ.
774 Sci. Technol., 46, 9511–9518, https://doi.org/10.1021/es301993s, 2012.
775 Hersbach, H., Bell, B., Berrisford, P., Hirahara, S., Horányi, A., Muñoz-Sabater, J., Nicolas, J.,
776 Peubey, C., Radu, R., Schepers, D., Simmons, A., Soci, C., Abdalla, S., Abellan, X., Balsamo, G.,
777 Bechtold, P., Biavati, G., Bidlot, J., Bonavita, M., De Chiara, G., Dahlgren, P., Dee, D.,
778 Diamantakis, M., Dragani, R., Flemming, J., Forbes, R., Fuentes, M., Geer, A., Haimberger, L.,

779 Healy, S., Hogan, R. J., Hólm, E., Janisková, M., Keeley, S., Laloyaux, P., Lopez, P., Lupu, C.,
780 Radnoti, G., de Rosnay, P., Rozum, I., Vamborg, F., Villaume, S., and Thépaut, J. N.: The ERA5
781 global reanalysis, Q. J. R. Meteorol. Soc., 146, 1999–2049, https://doi.org/10.1002/qj.3803, 2020.
782 Hourdin, F. and Armengaud, A.: The Use of Finite-Volume Methods for Atmospheric Advection of
783 Trace Species. Part I: Test of Various Formulations in a General Circulation Model, Mon. Weather
784 Rev., 127, 822–837, https://doi.org/10.1175/1520-0493(1999)127<0822:TUOFVM>2.0.CO;2,
785 1999.
786 Hourdin, F., Musat, I., Bony, S., Braconnot, P., Codron, F., Dufresne, J. L., Fairhead, L., Filiberti,
787 M. A., Friedlingstein, P., Grandpeix, J. Y., Krinner, G., LeVan, P., Li, Z. X., and Lott, F.: The
788 LMDZ4 general circulation model: Climate performance and sensitivity to parametrized physics
789 with emphasis on tropical convection, Clim. Dyn., 27, 787–813, https://doi.org/10.1007/s00382-
790 006-0158-0, 2006.
791 Hoyle, C. R., Fuchs, C., Jarvinen, E., Saathoff, H., Dias, A., El Haddad, I., Gysel, M., Coburn, S.
792 C., Trostl, J., Hansel, A., Bianchi, F., Breitenlechner, M., Corbin, J. C., Craven, J., Donahue, N. M.,
793 Duplissy, J., Ehrhart, S., Frege, C., Gordon, H., Hoppel, N., Heinritzi, M., Kristensen, T. B.,
794 Molteni, U., Nichman, L., Pinterich, T., Prevôt, A. S. H., Simon, M., Slowik, J. G., Steiner, G.,
795 Tome, A., Vogel, A. L., Volkamer, R., Wagner, A. C., Wagner, R., Wexler, A. S., Williamson, C.,
796 Winkler, P. M., Yan, C., Amorim, A., Dommen, J., Curtius, J., Gallagher, M. W., Flagan, R. C.,
797 Hansel, A., Kirkby, J., Kulmala, M., Mohler, O., Stratmann, F., Worsnop, D. R., and Baltensperger,
798 U.: Aqueous phase oxidation of sulphur dioxide by ozone in cloud droplets, Atmos. Chem. Phys.,
799 16, 1693–1712, https://doi.org/10.5194/acp-16-1693-2016, 2016.
800 Huang, X., Ding, A., Gao, J., Zheng, B., Zhou, D., Qi, X., Tang, R., Wang, J., Ren, C., Nie, W.,
801 Chi, X., Xu, Z., Chen, L., Li, Y., Che, F., Pang, N., Wang, H., Tong, D., Qin, W., Cheng, W., Liu,
802 W., Fu, Q., Liu, B., Chai, F., Davis, S. J., Zhang, Q., and He, K.: Enhanced secondary pollution
803 offset reduction of primary emissions during COVID-19 lockdown in China, Natl. Sci. Rev., 8,
804 https://doi.org/10.1093/nsr/nwaa137, 2021.
805 Jackson, R. B., Friedlingstein, P., Quéré, C. Le, Abernethy, S., Andrew, R. M., Canadell, J. G.,
806 Ciais, P., Davis, S. J., Deng, Z., Liu, Z., Korsbakken, J. I., and Peters, G. P.: Global fossil carbon
807 emissions rebound near pre-COVID-19 levels, Environ. Res. Lett., 17,
808 https://doi.org/https://doi.org/10.1088/1748-9326/ac55b6, 2022.
809 Kean, A. J., Littlejohn, D., Ban-Weiss, G. A., Harley, R. A., Kirchstetter, T. W., and Lunden, M.
810 M.: Trends in on-road vehicle emissions of ammonia, Atmos. Environ., 43, 1565–1570,
811 https://doi.org/10.1016/j.atmosenv.2008.09.085, 2009.
812 Kharol, S. K., Shephard, M. W., McLinden, C. A., Zhang, L., Sioris, C. E., O'Brien, J. M., Vet, R.,
813 Cady-Pereira, K. E., Hare, E., Siemons, J., and Krotkov, N. A.: Dry Deposition of Reactive

Nitrogen From Satellite Observations of Ammonia and Nitrogen Dioxide Over North America, Geophys. Res. Lett., 45, 1157–1166, https://doi.org/10.1002/2017GL075832, 2018.
Kirkby, J., Duplissy, J., Sengupta, K., Frege, C., Gordon, H., Williamson, C., Heinritzi, M., Simon, M., Yan, C., Almeida, J., Trostl, J., Nieminen, T., Ortega, I. K., Wagner, R., Adamov, A., Amorim, A., Bernhammer, A. K., Bianchi, F., Breitenlechner, M., Brilke, S., Chen, X., Craven, J., Dias, A., Ehrhart, S., Flagan, R. C., Franchin, A., Fuchs, C., Guida, R., Hakala, J., Hoyle, C. R., Jokinen, T., Junninen, H., Kangasluoma, J., Kim, J., Krapf, M., Kurten, A., Laaksonen, A., Lehtipalo, K., Makhmutov, V., Mathot, S., Molteni, U., Onnela, A., Perakyla, O., Piel, F., Petaja, T., Praplan, A. P., Pringle, K., Rap, A., Richards, N. A. D., Riipinen, I., Rissanen, M. P., Rondo, L., Sarnela, N., Schobesberger, S., Scott, C. E., Seinfeld, J. H., Sipila, M., Steiner, G., Stozhkov, Y., Stratmann, F., Tomé, A., Virtanen, A., Vogel, A. L., Wagner, A. C., Wagner, P. E., Weingartner, E., Wimmer, D., Winkler, P. M., Ye, P., Zhang, X., Hansel, A., Dommen, J., Donahue, N. M., Worsnop, D. R., Baltensperger, U., Kulmala, M., Carslaw, K. S., and Curtius, J.: Ion-induced nucleation of pure biogenic particles, Nature, 533, 521–526, https://doi.org/10.1038/nature17953, 2016.
Klimont, Z.: personal communication, 2022.
Klimont, Z., Kupiainen, K., Heyes, C., Purohit, P., Cofala, J., Rafaj, P., Borken-Kleefeld, J., and Schöpp, W.: Global anthropogenic emissions of particulate matter including black carbon, Atmos. Chem. Phys., 17, 8681–8723, https://doi.org/10.5194/acp-17- 50 8681-2017, 2017.
Krinner, G., Viovy, N., de Noblet-Ducoudré, N., Ogée, J., Polcher, J., Friedlingstein, P., Ciais, P., Sitch, S., and Prentice, I. C.: A dynamic global vegetation model for studies of the coupled atmosphere-biosphere system, Global Biogeochem. Cycles, 19, GB1015, https://doi.org/10.1029/2003GB002199, 2005.
Kristiansen, N. I., Stohl, A., Olivié, D. J. L., Croft, B., Søvde, O. A., Klein, H., Christoudias, T., Kunkel, D., Leadbetter, S. J., Lee, Y. H., Zhang, K., Tsigaridis, K., Bergman, T., Evangeliou, N., Wang, H., Ma, P. L., Easter, R. C., Rasch, P. J., Liu, X., Pitari, G., Di Genova, G., Zhao, S. Y., Balkanski, Y., Bauer, S. E., Faluvegi, G. S., Kokkola, H., Martin, R. V., Pierce, J. R., Schulz, M., Shindell, D., Tost, H., and Zhang, H.: Evaluation of observed and modelled aerosol lifetimes using radioactive tracers of opportunity and an ensemble of 19 global models, 3525–3561 pp., https://doi.org/10.5194/acp-16-3525-2016, 2016.
Krupa, S. V.: Effects of atmospheric ammonia (NH3) on terrestrial vegetation: A review, Environ. Pollut., 124, 179–221, https://doi.org/10.1016/S0269-7491(02)00434-7, 2003.
Kuttippurath, J., Patel, V. K., Kashyap, R., Singh, A., and Clerbaux, C.: Anomalous increase in global atmospheric ammonia during COVID-19 lockdown: Need for policies to curb agricultural emissions, J. Clean. Prod., 434, 140424, https://doi.org/10.1016/j.jclepro.2023.140424, 2023.
Lachatre, M., Fortems-Cheiney, A., Foret, G., Siour, G., Dufour, G., Clarisse, L., Clerbaux, C.,

Coheur, P. F., Van Damme, M., and Beekmann, M.: The unintended consequence of SO2 and NO2 regulations over China: Increase of ammonia levels and impact on PM2.5 concentrations, Atmos. Chem. Phys., 19, 6701–6716, https://doi.org/10.5194/acp-19-6701-2019, 2019.

Le, T., Wang, Y., Liu, L., Yang, J., Yung, Y. L., Li, G., and Seinfeld, J. H.: Unexpected air pollution with marked emission reductions during the COVID-19 outbreak in China, Science (80-.)., eabb7431, https://doi.org/10.1126/science.abb7431, 2020.

Lelieveld, J., Evans, J. S., Fnais, M., Giannadaki, D., and Pozzer, A.: The contribution of outdoor air pollution sources to premature mortality on a global scale., Nature, 525, 367–71, https://doi.org/10.1038/nature15371, 2015.

Leung, D. M., Shi, H., Zhao, B., Wang, J., Ding, E. M., Gu, Y., Zheng, H., Chen, G., Liou, K. N., Wang, S., Fast, J. D., Zheng, G., Jiang, J., Li, X., and Jiang, J. H.: Wintertime Particulate Matter Decrease Buffered by Unfavorable Chemical Processes Despite Emissions Reductions in China, Geophys. Res. Lett., 47, 1–12, https://doi.org/10.1029/2020GL087721, 2020.

Li, B., Ma, Y., Zhou, Y., and Chai, E.: Research progress of different components of PM2.5 and ischemic stroke, Sci. Rep., 13, 1–12, https://doi.org/10.1038/s41598-023-43119-5, 2023.

Li, C., Martin, R. V, Shephard, M. W., Pereira, K. C., Cooper, M. J., Kaiser, J., Lee, C. J., Zhang, L., and Henze, D. K.: Assessing the Iterative Finite Difference Mass Balance and 4D - Var Methods to Derive Ammonia Emissions Over North America Using Synthetic Observations, J. Geophys. Res. Atmos., 124, 4222–4236, https://doi.org/10.1029/2018JD030183, 2019.

Li, L., Li, Q., Huang, L., Wang, Q., Zhu, A., Xu, J., Liu, Z., Li, H., Shi, L., Li, R., Azari, M., Wang, Y., Zhang, X., Liu, Z., Zhu, Y., Zhang, K., Xue, S., Ooi, M. C. G., Zhang, D., and Chan, A.: Air quality changes during the COVID-19 lockdown over the Yangtze River Delta Region: An insight into the impact of human activity pattern changes on air pollution variation, Sci. Total Environ., 732, https://doi.org/10.1016/j.scitotenv.2020.139282, 2020.

Liu, L., Li, H., Zhang, H., Zhong, J., Bai, Y., Ge, M., Li, Z., Chen, Y., and Zhang, X.: The role of nitric acid in atmospheric new particle formation, Phys. Chem. Chem. Phys., 20, 17406–17414, https://doi.org/10.1039/C8CP02719F, 2018.

Lovarelli, D., Fugazza, D., Costantini, M., Conti, C., Diolaiuti, G., and Guarino, M.: Comparison of ammonia air concentration before and during the spread of COVID-19 in Lombardy (Italy) using ground-based and satellite data, Atmos. Environ., 259, 118534, https://doi.org/10.1016/j.atmosenv.2021.118534, 2021.

Malm, W. C.: Spatial and monthly trends in speciated fine particle concentration in the United States, J. Geophys. Res., 109, D03306, https://doi.org/10.1029/2003JD003739, 2004.

Matthias, V., Quante, M., Arndt, J. A., Badeke, R., Fink, L., Petrik, R., Feldner, J., Schwarzkopf, D., Link, E. M., Ramacher, M. O. P., and Wedemann, R.: The role of emission reductions and the

meteorological situation for air quality improvements during the COVID-19 lockdown period in central Europe, Atmos. Chem. Phys., 21, 13931–13971, https://doi.org/10.5194/acp-21-13931-2021, 2021.

Mo, Z., Huang, J., Chen, Z., Zhou, B., Zhu, K., Liu, H., Mu, Y., Zhang, D., and Wang, S.: Cause analysis of PM2.5 pollution during the COVID-19 lockdown in Nanning, China, Sci. Rep., 11, 1–13, https://doi.org/10.1038/s41598-021-90617-5, 2021.

Pai, S. J., Heald, C. L., and Murphy, J. G.: Exploring the Global Importance of Atmospheric Ammonia Oxidation, ACS Earth Sp. Chem., 5, 1674–1685, https://doi.org/10.1021/acsearthspacechem.1c00021, 2021.

Patel, H., Talbot, N., Salmond, J., Dirks, K., Xie, S., and Davy, P.: Implications for air quality management of changes in air quality during lockdown in Auckland (New Zealand) in response to the 2020 SARS-CoV-2 epidemic, Sci. Total Environ., 746, 141129, https://doi.org/10.1016/j.scitotenv.2020.141129, 2020.

Paulot, F., Jacob, D. J., Pinder, R. W., Bash, J. O., Travis, K., and Henze, D. K.: Ammonia emissions in the United States, European Union, and China derived by high-resolution inversion of ammonium wet deposition data: Interpretation with a new agricultural emissions inventory (MASAGE-NH3), J. Geophys. Res. Atmos., 119, 4343–4364, https://doi.org/10.1002/2013JD021130, 2014.

Pisso, I., Sollum, E., Grythe, H., Kristiansen, N., Cassiani, M., Eckhardt, S., Arnold, D., Morton, D., Thompson, R. L., Groot Zwaaftink, C. D., Evangeliou, N., Sodemann, H., Haimberger, L., Henne, S., Brunner, D., Burkhart, J. F., Fouilloux, A., Brioude, J., Philipp, A., Seibert, P., and Stohl, A.: The Lagrangian particle dispersion model FLEXPART version 10.4, Geosci. Model Dev., 12, 4955–4997, https://doi.org/10.5194/gmd-12-4955-2019, 2019.

Pope, C. A. and Dockery, D. W.: Health effects of fine particulate air pollution: Lines that connect, J. Air Waste Manag. Assoc., 56, 709–742, https://doi.org/10.1080/10473289.2006.10464485, 2006.

Pope III, C. A., Burnett, R. T., Thun, M. J., Calle, E. E., Krewski, D., and Thurston, G. D.: Lung Cancer, Cardiopulmonary Mortality, and Long-term Exposure to Fine Particulate Air Pollution, J. Am. Med. Assoc., 287, 1132–1141, https://doi.org/10.1001/jama.287.9.1132, 2002.

Pozzer, A., Tsimpidi, A. P., Karydis, V. A., De Meij, A., and Lelieveld, J.: Impact of agricultural emission reductions on fine-particulate matter and public health, Atmos. Chem. Phys., 17, 12813–12826, https://doi.org/10.5194/acp-17-12813-2017, 2017.

Putaud, J. P., Pozzoli, L., Pisoni, E., Martins Dos Santos, S., Lagler, F., Lanzani, G., Dal Santo, U., and Colette, A.: Impacts of the COVID-19 lockdown on air pollution at regional and urban background sites in northern Italy, Atmos. Chem. Phys., 21, 7597–7609, https://doi.org/10.5194/acp-21-7597-2021, 2021.

Putaud, J. P., Pisoni, E., Mangold, A., Hueglin, C., Sciare, J., Pikridas, M., Savvides, C., Ondracek, J., Mbengue, S., Wiedensohler, A., Weinhold, K., Merkel, M., Poulain, L., Van Pinxteren, D., Herrmann, H., Massling, A., Nordstroem, C., Alastuey, A., Reche, C., Pérez, N., Castillo, S., Sorribas, M., Adame, J. A., Petaja, T., Lehtipalo, K., Niemi, J., Riffault, V., De Brito, J. F., Colette, A., Favez, O., Petit, J. E., Gros, V., Gini, M. I., Vratolis, S., Eleftheriadis, K., Diapouli, E., Denier Van Der Gon, H., Yttri, K. E., and Aas, W.: Impact of 2020 COVID-19 lockdowns on particulate air pollution across Europe, Atmos. Chem. Phys., 23, 10145–10161, https://doi.org/10.5194/acp-23-10145-2023, 2023.

Querol, X., Massagué, J., Alastuey, A., Moreno, T., Gangoiti, G., Mantilla, E., Duéguez, J. J., Escudero, M., Monfort, E., Pérez García-Pando, C., Petetin, H., Jorba, O., Vázquez, V., de la Rosa, J., Campos, A., Muñóz, M., Monge, S., Hervás, M., Javato, R., and Cornide, M. J.: Lessons from the COVID-19 air pollution decrease in Spain: Now what?, Sci. Total Environ., 779, https://doi.org/10.1016/j.scitotenv.2021.146380, 2021.

Reche, C., Viana, M., Pandolfi, M., Alastuey, A., Moreno, T., Amato, F., Ripoll, A., and Querol, X.: Urban NH 3 levels and sources in a Mediterranean environment, Atmos. Environ., 57, 153–164, https://doi.org/10.1016/j.atmosenv.2012.04.021, 2012.

Rennie, S., Watkins, J., Ball, L., Brown, M., Fry, M., Henrys, P., Hollaway, M., Quinn, J., Sier, A., and Dick, J.: Shaping the development of the UKCEH UK-SCAPE Data Science Framework. Workshop report, 2020.

Rodgers, C. D.: Inverse Methods for Atmospheric Sounding, WORLD SCIENTIFIC, 256 pp., https://doi.org/doi:10.1142/3171, 2000.

Schobesberger, S., Franchin, A., Bianchi, F., Rondo, L., Duplissy, J., Kürten, A., Ortega, I. K., Metzger, A., Schnitzhofer, R., Almeida, J., Amorim, A., Dommen, J., Dunne, E. M., Ehn, M., Gagné, S., Ickes, L., Junninen, H., Hansel, A., Kerminen, V. M., Kirkby, J., Kupc, A., Laaksonen, A., Lehtipalo, K., Mathot, S., Onnela, A., Petäjä, T., Riccobono, F., Santos, F. D., Sipilä, M., Tomé, A., Tsagkogeorgas, G., Viisanen, Y., Wagner, P. E., Wimmer, D., Curtius, J., Donahue, N. M., Baltensperger, U., Kulmala, M., and Worsnop, D. R.: On the composition of ammonia-sulfuric-acid ion clusters during aerosol particle formation, Atmos. Chem. Phys., 15, 55–78, https://doi.org/10.5194/acp-15-55-2015, 2015.

Seinfeld, J. H. and Pandis, S. N.: Atmospheric Chemistry and Physics. From Air Pollution to Climate Change, 2nd ed., John Wiley & Sons, NY, 2000.

Shephard, M. W. and Cady-Pereira, K. E.: Cross-track Infrared Sounder (CrIS) satellite observations of tropospheric ammonia, Atmos. Meas. Tech., 8, 1323–1336, https://doi.org/10.5194/amt-8-1323-2015, 2015.

Shephard, M. W., McLinden, C. A., Cady-Pereira, K. E., Luo, M., Moussa, S. G., Leithead, A.,

954 Liggio, J., Staebler, R. M., Akingunola, A., Makar, P., Lehr, P., Zhang, J., Henze, D. K., Millet, D.
955 B., Bash, J. O., Zhu, L., Wells, K. C., Capps, S. L., Chaliyakunnel, S., Gordon, M., Hayden, K.,
956 Brook, J. R., Wolde, M., and Li, S. M.: Tropospheric Emission Spectrometer (TES) satellite
957 observations of ammonia, methanol, formic acid, and carbon monoxide over the Canadian oil sands:
958 Validation and model evaluation, Atmos. Meas. Tech., 8, 5189–5211, https://doi.org/10.5194/amt-
959 8-5189-2015, 2015.
960 Shephard, M. W., Dammers, E., E. Cady-Pereira, K., K. Kharol, S., Thompson, J., Gainariu-Matz,
961 Y., Zhang, J., A. McLinden, C., Kovachik, A., Moran, M., Bittman, S., E. Sioris, C., Griffin, D., J.
962 Alvarado, M., Lonsdale, C., Savic-Jovcic, V., and Zheng, Q.: Ammonia measurements from space
963 with the Cross-track Infrared Sounder: Characteristics and applications, Atmos. Chem. Phys., 20,
964 2277–2302, https://doi.org/10.5194/acp-20-2277-2020, 2020.
965 Shi, X. and Brasseur, G. P.: The Response in Air Quality to the Reduction of Chinese Economic
966 Activities During the COVID-19 Outbreak, Geophys. Res. Lett., 47, 1–8,
967 https://doi.org/10.1029/2020GL088070, 2020.
968 Shi, Z., Song, C., Liu, B., Lu, G., Xu, J., Van Vu, T., Elliott, R. J. R., Li, W., Bloss, W. J., and
969 Harrison, R. M.: Abrupt but smaller than expected changes in surface air quality attributable to
970 COVID-19 lockdowns, Sci. Adv., 7, https://doi.org/10.1126/sciadv.abd6696, 2021.
971 Sicard, P., De Marco, A., Agathokleous, E., Feng, Z., Xu, X., Paoletti, E., Rodriguez, J. J. D., and
972 Calatayud, V.: Amplified ozone pollution in cities during the COVID-19 lockdown, Sci. Total
973 Environ., 735, https://doi.org/10.1016/j.scitotenv.2020.139542, 2020.
974 Sitwell, M., Shephard, M., Rochon, Y., Cady-Pereira, K., and Dammers, E.: An Ensemble-
975 Variational Inversion System for the Estimation of Ammonia Emissions using CrIS Satellite
976 Ammonia Retrievals, 22, 6595–6624, https://doi.org/10.5194/acp-22-6595-2022, 2022.
977 Sohrabi, C., Alsafi, Z., O'Neill, N., Khan, M., Kerwan, A., Al-Jabir, A., Iosifidis, C., and Agha, R.:
978 World Health Organization declares global emergency: A review of the 2019 novel coronavirus
979 (COVID-19), Int. J. Surg., 76, 71–76, https://doi.org/10.1016/j.ijsu.2020.02.034, 2020.
980 Sørensen, L. L., Hertel, O., Skjøth, C. A., Lund, M., and Pedersen, B.: Fluxes of ammonia in the
981 coastal marine boundary layer, Atmos. Environ., 37, 167–177, https://doi.org/10.1016/S1352-
982 2310(03)00247-4, 2003.
983 Stevens, C. J., Dupr, C., Dorland, E., Gaudnik, C., Gowing, D. J. G., Bleeker, A., Diekmann, M.,
984 Alard, D., Bobbink, R., Fowler, D., Corcket, E., Mountford, J. O., Vandvik, V., Aarrestad, P. A.,
985 Muller, S., and Dise, N. B.: Nitrogen deposition threatens species richness of grasslands across
986 Europe, Environ. Pollut., 158, 2940–2945, https://doi.org/10.1016/j.envpol.2010.06.006, 2010.
987 Stohl, A., Forster, C., Frank, A., Seibert, P., and Wotawa, G.: Technical note: The Lagrangian
988 particle dispersion model FLEXPART version 6.2, Atmos. Chem. Phys., 5, 2461–2474,

https://doi.org/10.5194/acp-5-2461-2005, 2005.
Sutton, M. A., Dragosits, U., Tang, Y. S., and Fowler, D.: Ammonia emissions from non-agricultural sources in the UK, 34, 2000a.
Sutton, M. A., Dragosits, U., Tang, Y. S., and Fowler, D.: Ammonia emissions from non-agricultural sources in the UK, Atmos. Environ., 34, 855–869, 2000b.
Sutton, M. A., Erisman, J. W., Dentener, F., and Möller, D.: Ammonia in the environment: From ancient times to the present, Environ. Pollut., 156, 583–604, https://doi.org/10.1016/j.envpol.2008.03.013, 2008.
Sutton, M. A., Reis, S., Riddick, S. N., Dragosits, U., Nemitz, E., Theobald, M. R., Tang, Y. S., Braban, C. F., Vieno, M., Dore, A. J., Mitchell, R. F., Wanless, S., Daunt, F., Fowler, D., Blackall, T. D., Milford, C., Flechard, C. R., Loubet, B., Massad, R., Cellier, P., Personne, E., Coheur, P. F., Clarisse, L., Damme, M. Van, Ngadi, Y., Clerbaux, C., Skjøth, C. A., Geels, C., Hertel, O., Kruit, R. J. W., Pinder, R. W., Bash, J. O., Walker, J. T., Simpson, D., Horvath, L., Misselbrook, T. H., Bleeker, A., Dentener, F., and Vries, W. de: Towards a climate-dependent paradigm of ammonia emission and deposition, Philos. Trans. R. Soc. B Biol. Sci., 368, 20130166–20130166, https://doi.org/10.1098/rstb.2013.0166, 2013.
Szczepańska, A. and Pietrzyka, K.: The COVID-19 epidemic in Poland and its influence on the quality of life of university students (young adults) in the context of restricted access to public spaces, J. Public Heal., https://doi.org/10.1007/s10389-020-01456-z, 2021.
Thunis, P., Clappier, A., Beekmann, M., Putaud, J. P., Cuvelier, C., Madrazo, J., and De Meij, A.: Non-linear response of PM2.5 to changes in NOx and NH3 emissions in the Po basin (Italy): Consequences for air quality plans, Atmos. Chem. Phys., 21, 9309–9327, https://doi.org/10.5194/acp-21-9309-2021, 2021.
Tichý, O., Šmídl, V., Hofman, R., and Stohl, A.: LS-APC v1.0: A tuning-free method for the linear inverse problem and its application to source-Term determination, Geosci. Model Dev., 9, 4297–4311, https://doi.org/10.5194/gmd-9-4297-2016, 2016.
Tichý, O., Ulrych, L., Šmídl, V., Evangeliou, N., and Stohl, A.: On the tuning of atmospheric inverse methods: Comparisons with the European Tracer Experiment (ETEX) and Chernobyl datasets using the atmospheric transport model FLEXPART, Geosci. Model Dev., 13, 5917–5934, https://doi.org/10.5194/gmd-13-5917-2020, 2020.
Tichý, O., Eckhardt, S., Balkanski, Y., Hauglustaine, D., and Evangeliou, N.: Decreasing trends of ammonia emissions over Europe seen from remote sensing and inverse modelling, Atmos. Chem. Phys., 23, 15235–15252, https://doi.org/10.5194/acp-23-15235-2023, 2023.
Varotsos, C., Christodoulakis, J., Kouremadas, G. A., and Fotaki, E. F.: The Signature of the Coronavirus Lockdown in Air Pollution in Greece, Water. Air. Soil Pollut., 232,

https://doi.org/10.1007/s11270-021-05055-w, 2021.
Viatte, C., Petit, J. E., Yamanouchi, S., Van Damme, M., Doucerain, C., Germain-Piaulenne, E., Gros, V., Favez, O., Clarisse, L., Coheur, P. F., Strong, K., and Clerbaux, C.: Ammonia and pm2.5 air pollution in paris during the 2020 covid lockdown, Atmosphere (Basel)., 12, 1–18, https://doi.org/10.3390/atmos12020160, 2021.
De Vries, W., Kros, J., Reinds, G. J., and Butterbach-Bahl, K.: Quantifying impacts of nitrogen use in European agriculture on global warming potential, Curr. Opin. Environ. Sustain., 3, 291–302, https://doi.org/10.1016/j.cosust.2011.08.009, 2011.
Walters, W. W., Chai, J., and Hastings, M. G.: Theoretical Phase Resolved Ammonia-Ammonium Nitrogen Equilibrium Isotope Exchange Fractionations: Applications for Tracking Atmospheric Ammonia Gas-to-Particle Conversion, ACS Earth Sp. Chem., 3, 79–89, https://doi.org/10.1021/acsearthspacechem.8b00140, 2019.
Wang, M., Xiao, M., Bertozzi, B., Marie, G., Rörup, B., Schulze, B., Bardakov, R., He, X. C., Shen, J., Scholz, W., Marten, R., Dada, L., Baalbaki, R., Lopez, B., Lamkaddam, H., Manninen, H. E., Amorim, A., Ataei, F., Bogert, P., Brasseur, Z., Caudillo, L., De Menezes, L. P., Duplissy, J., Ekman, A. M. L., Finkenzeller, H., Carracedo, L. G., Granzin, M., Guida, R., Heinritzi, M., Hofbauer, V., Höhler, K., Korhonen, K., Krechmer, J. E., Kürten, A., Lehtipalo, K., Mahfouz, N. G. A., Makhmutov, V., Massabò, D., Mathot, S., Mauldin, R. L., Mentler, B., Müller, T., Onnela, A., Petäjä, T., Philippov, M., Piedehierro, A. A., Pozzer, A., Ranjithkumar, A., Schervish, M., Schobesberger, S., Simon, M., Stozhkov, Y., Tomé, A., Umo, N. S., Vogel, F., Wagner, R., Wang, D. S., Weber, S. K., Welti, A., Wu, Y., Zauner-Wieczorek, M., Sipilä, M., Winkler, P. M., Hansel, A., Baltensperger, U., Kulmala, M., Flagan, R. C., Curtius, J., Riipinen, I., Gordon, H., Lelieveld, J., El-Haddad, I., Volkamer, R., Worsnop, D. R., Christoudias, T., Kirkby, J., Möhler, O., and Donahue, N. M.: Synergistic HNO3–H2SO4–NH3 upper tropospheric particle formation, Nature, 605, 483–489, https://doi.org/10.1038/s41586-022-04605-4, 2022.
Wang, P., Chen, K., Zhu, S., Wang, P., and Zhang, H.: Severe air pollution events not avoided by reduced anthropogenic activities during COVID-19 outbreak, Resour. Conserv. Recycl., 158, 104814, https://doi.org/10.1016/j.resconrec.2020.104814, 2020.
Weber, R. J., McMurry, P. H., Mauldin, R. L., Tanner, D. J., Eisele, F. L., Clarke, A. D., and Kapustin, V. N.: New particle formation in the remote troposphere: A comparison of observations at various sites, Geophys. Res. Lett., 26, 307–310, https://doi.org/10.1029/1998GL900308, 1999.
White, E., Shephard, M. W., Cady-Pereira, K. E., Kharol, S. K., Ford, S., Dammers, E., Chow, E., Thiessen, N., Tobin, D., Quinn, G., O'Brien, J., and Bash, J.: Accounting for Non-Detects: Application to Satellite Ammonia Observations, Remote Sens., 15, https://doi.org/10.3390/rs15102610, 2023.

Xu, W., Zhao, Y., Wen, Z., Chang, Y., Pan, Y., Sun, Y., and Ma, X.: Increasing importance of ammonia emission abatement in PM2.5 pollution control, Sci. Bull., 67, 1745–1749, https://doi.org/10.1016/j.scib.2022.07.021, 2022.

Zavyalov, V., Esplin, M., Scott, D., Esplin, B., Bingham, G., Hoffman, E., Lietzke, C., Predina, J., Frain, R., Suwinski, L., Han, Y., Major, C., Graham, B., and Phillips, L.: Noise performance of the CrIS instrument, J. Geophys. Res. Atmos., 118, 108–120, https://doi.org/10.1002/2013JD020457, 2013.

Zhai, S., Jacob, D. J., Wang, X., Liu, Z., Wen, T., Shah, V., Li, K., Moch, J. M., Bates, K. H., Song, S., Shen, L., Zhang, Y., Luo, G., Yu, F., Sun, Y., Wang, L., Qi, M., Tao, J., Gui, K., Xu, H., Zhang, Q., Zhao, T., Wang, Y., Lee, H. C., Choi, H., and Liao, H.: Control of particulate nitrate air pollution in China, Nat. Geosci., 14, 389–395, https://doi.org/10.1038/s41561-021-00726-z, 2021.

Zhang, X., Zhang, Z., Xiao, Z., Tang, G., Li, H., Gao, R., Dao, X., Wang, Y., and Wang, W.: Heavy haze pollution during the COVID-19 lockdown in the Beijing-Tianjin-Hebei region, China, J. Environ. Sci. (China), 114, 170–178, https://doi.org/10.1016/j.jes.2021.08.030, 2022.

Zhang, Y., Zhang, C., Liu, Z., and Yang, X.: Air pollution reduction during COVID-19 lockdown in China: a sustainable impact assessment for future cities development, City Built Environ., 1, 1–21, https://doi.org/10.1007/s44213-023-00013-0, 2023.

FIGURE LEGENDS

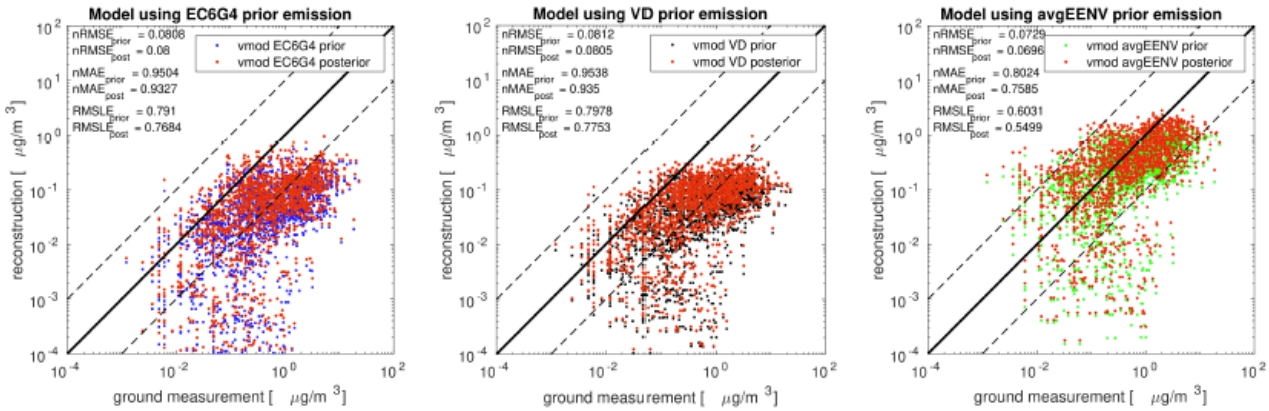

Figure 1. Scatter plots of prior and posterior concentrations against independent observations (observations that were not included in the inversion algorithm) from the EMEP network (https://emep.int/mscw/, **Figure S 1**) from January to July 2020. Three statistical measures (nRMSE, nMAE and RMSLE) were used to assess the performance of each inversion using three different prior emission inventories for ammonia (EC6G4, VD and avgEENV).

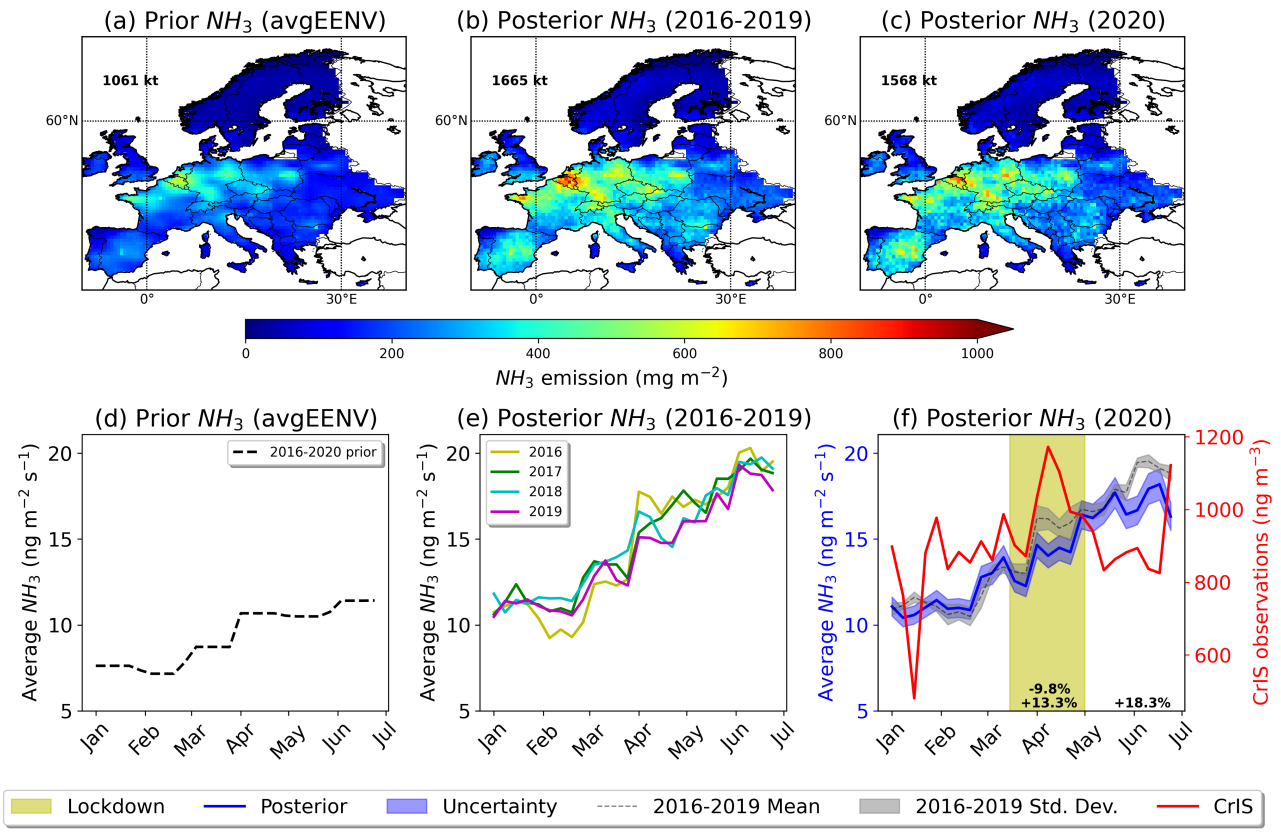

Figure 2. (a) Total a priori emissions of ammonia over Europe for the inversion period (January – June). The emissions correspond to avgEENV prior, and the total emitted amount is equal to 1061 kt. (b) Total a posteriori emissions of ammonia over Europe for the inversion period (January – June) for the reference period 2016 – 2019 (using avgEENV prior) that amount 1665 kt. (c) Total posterior emissions of ammonia over Europe for January – June 2020 (1568 kt) using the avgEENV as the prior. (d) Timeseries of weekly-average prior emissions of ammonia over Europe (January to June 2020) from avgEENV prior. (e) Timeseries of weekly-average posterior emissions of ammonia over Europe for the reference years 2016–2019 (January to June) (yellow, green, cyan, magenta colors). (f) Timeseries of weekly-average posterior emissions of ammonia with the associated uncertainties over Europe in 2020 resulting from inversions using the avgEENV prior are plotted together with the CrIS observations averaged over Europe (red line) and the mean ammonia emissions with the calculated standard deviations for the reference period (2016–2019). The single top number -9.8% shows percentage change in ammonia emissions during the 2020 lockdown as compared to the same period in reference years, whereas two bottom ones show the corresponding changes in ammonia emissions (i) during the 2020 lockdown as compared to the period before lockdown (+13.3%), and (ii) the period after lockdown finished as compared to the lockdown period +18.3%), known as rebound period.

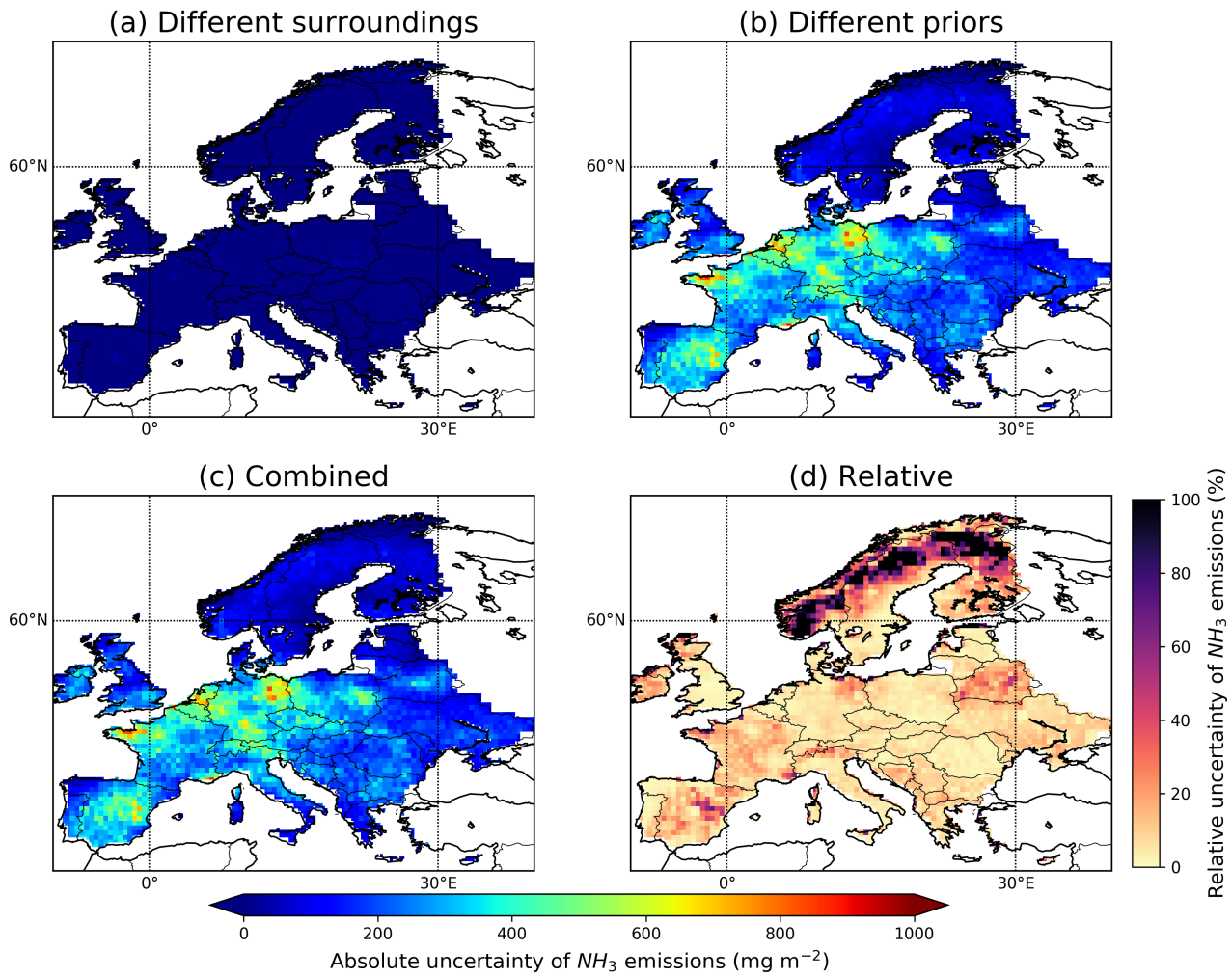

Figure 3. (a) Absolute uncertainty from use of different surrounding grid area for each spatial element of our inversion domain in the sensitivity tests; 2° to 4° grid-cells were considered resulting in a mean relative uncertainty of 4%. (b) Absolute uncertainty from use of four different prior emission estimates, namely EC6G4, VD, EGG and NE (see section 2.3). Here, a much larger uncertainty was calculated, due to the use of tenfold different prior emission datasets. (c) Propagated absolute uncertainty from the different sensitivity tests, and (d) relative uncertainty with respect to the posterior emissions (**Figure 2**c). The average uncertainty in the inversion domain for the first half of 2020 was estimated to be 11%.

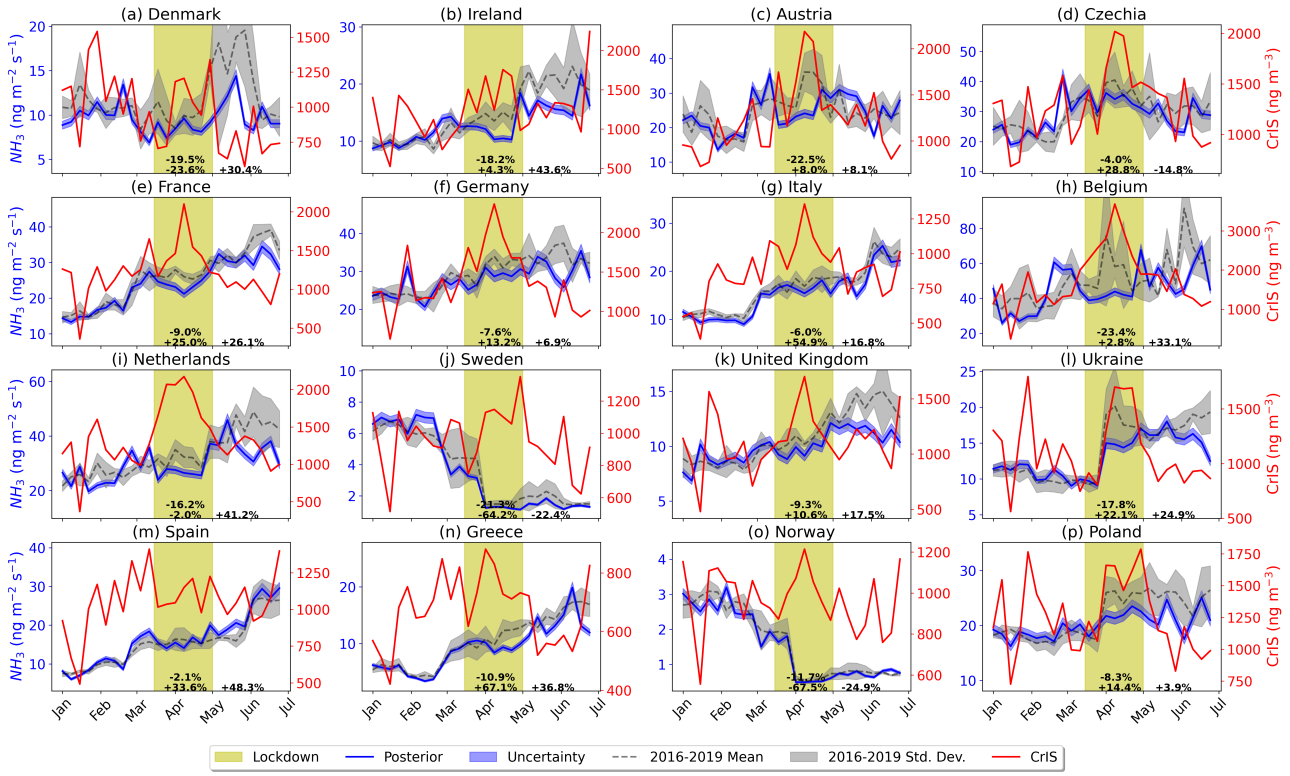

Figure 4. Timeseries of weekly-average posterior emissions of ammonia with the calculated uncertainties in different European countries in 2020 resulting from inversions using prior information from avgEENV plotted together with the CrIS observations averaged over Europe (red line) and mean emissions with the calculated standard deviations for the reference period (2016–2019). The single top numbers show the change in ammonia emissions during the 2020 lockdowns (15 March – 30 April) as compared to the same period the years before (2016-2019), whereas the two bottom ones show the respective changes in ammonia emissions during the 2020 lockdown as compared to the period before the lockdown, and after lockdown finished compared to the lockdown period (rebound period).

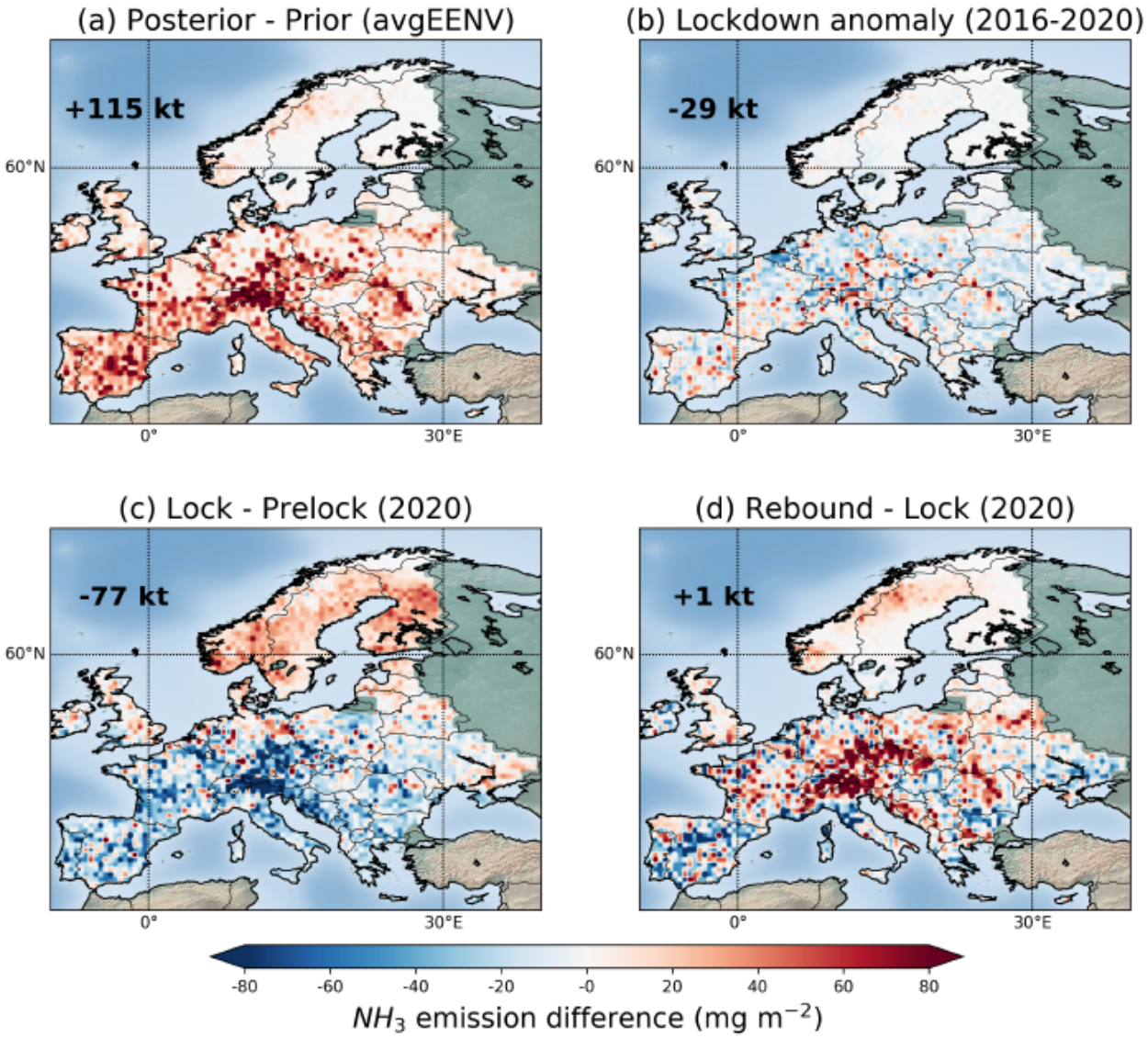

Figure 5. (a) Difference of posterior from prior emissions of ammonia during the European lockdowns of 2020 (15 March – 30 April) using the avgEENV emissions as the prior. (b) Emission anomaly relative to the 2020 lockdowns from the 2016-2020 period (15 March – 30 April). Difference in posterior ammonia (c) during the 2020 lockdowns (15 March – 30 April, Lock) from the period before (1 January – 14 March) and (d) after the 2020 lockdowns (1 May – 31 June, Reb) from the period during the 2020 lockdowns (15 March – 30 April, Lock) compared with the reference years (2016–2019).

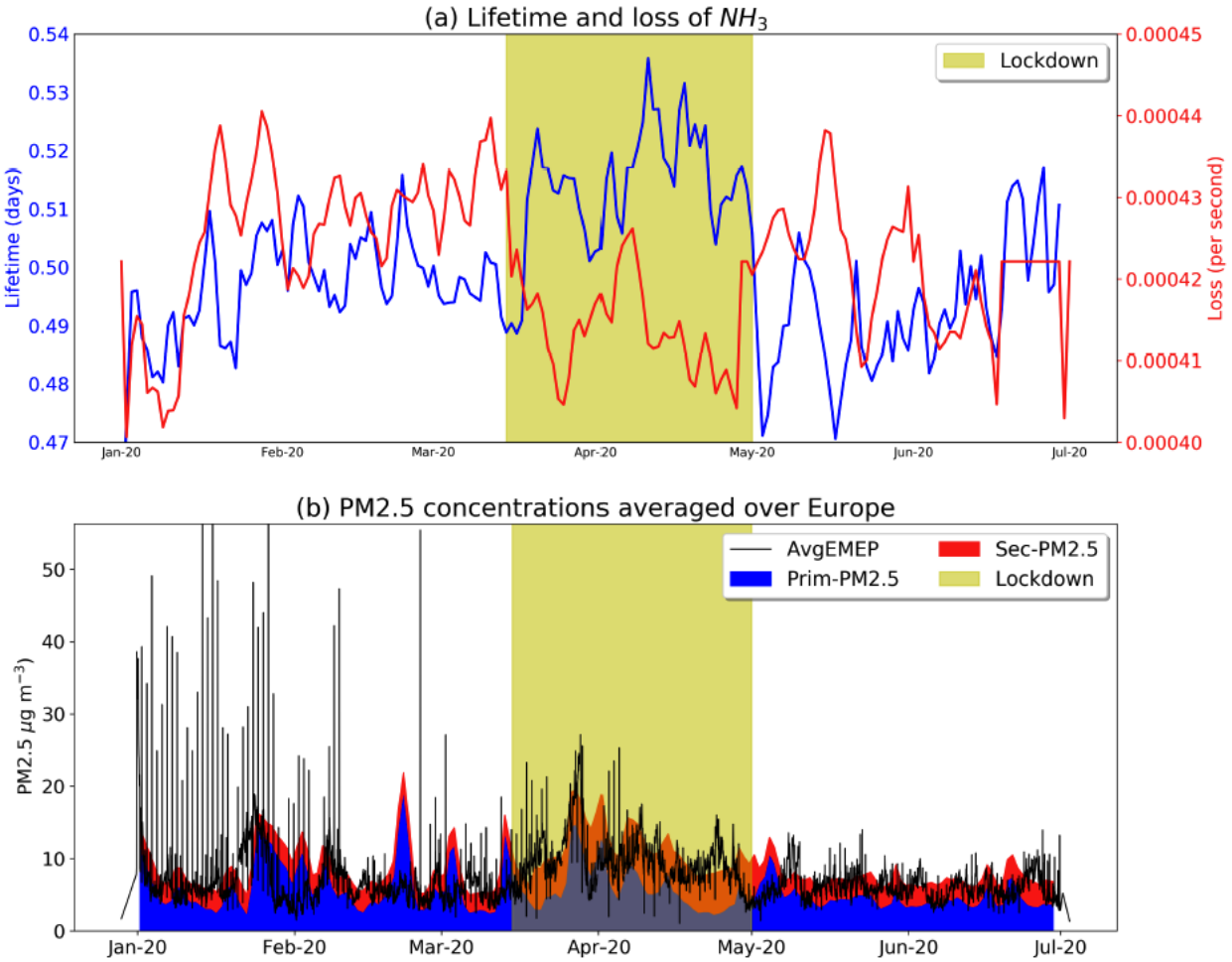

Figure 6. (a) Modelled lifetime (blue) and loss-rates (red) of atmospheric ammonia averaged over Europe for January – June 2020. The lockdown period (15 March – 30 April) is shaded in yellow. Right after COVID-19 restrictions were applied, loss-rates of ammonia (shown in red) were disturbed due to reported decreases on SO_2 and NO_x (Guevara et al., 2021; Doumbia et al., 2021), precursors of sulfuric and nitric acids (with which ammonia reacts to form PM2.5) and the constant accumulation of atmospheric ammonia. This had an effect on the lifetime of ammonia (plotted in blue), which started increasing in Europe leading to further accumulation of ammonia. (b) Observations of PM2.5 from the EMEP stations (78 stations) plotted against modelled PM2.5 concentrations, both averaged over Europe, from primary sources and secondary formation. It is evident that right after lockdown (yellow shade), secondary PM2.5 formation maintained high concentrations across Europe.